INFRARED SURFACE PLASMON POLARITONS ON SEMICONDUCTOR, SEMIMETAL AND CONDUCTING POLYMER

by

MONAS SHAHZAD
M.Sc. Government College Lahore, 2001
M.S. University of Central Florida, 2010

A dissertation submitted in partial fulfillment of the requirements
for the degree of Doctor of Philosophy
in the Department of Physics
in the College of Sciences
at the University of Central Florida
Orlando, Florida

Fall Term
2012

Major Professor: Robert E. Peale

ABSTRACT

Conductors with IR (infrared) plasma frequencies are potentially useful hosts of surface plasmon polaritons (SPPs) with subwavelength mode confinement for sensing applications. The underlying aim of this work is to identify such conductors that also have sharp SPP excitation resonances for biosensor applications at infrared (3-11 μm) wavelengths, where biological analytes are strongly differentiated by their IR absorption spectra. In this work, various materials were investigated such as a heavily doped semiconductor, a semimetal, a conducting polymer and its composite.

Heavily doped silicon was investigated by tuning its plasma frequency to the infrared region by heavily doping. The measured complex permittivity spectra for p-type silicon with a carrier concentration of 6×10^{19} and 6×10^{20} cm^{-3} show that these materials support SPPs beyond 11 and 6 μm wavelengths, respectively. SPP generation was observed in angular reflection spectra of doped-silicon gratings. Photon-to-plasmon coupling resonances, a necessary condition for sensing, were demonstrated near 10 μm wavelength for the heaviest doped, and the observed resonances were confirmed theoretically using analytic calculations. The permittivity spectra were also used to calculate SPP mode heights above the silicon surface and SPP propagation lengths. Reasonable merit criteria applied to these quantities suggest that only the heaviest doped material has sensor potential, and then mainly within the wavelength range of 6 to 10 μm.

The semimetal bismuth (Bi) has an infrared plasmon frequency less than the infrared plasma frequency of noble metals such as gold and silver, which is one order of magnitude lower than their plasma frequencies. The excitation of IR surface plasmons on Bi lamellar gratings in the wavelength range of 3.4 μm to 10.6 μm was observed. Distinct SPP resonances were observed although the usual condition for bound SPP is not satisfied in this wavelength range because the real part of the permittivity is positive. The excitation of these resonances agrees theoretically with the electromagnetic surface waves called surface polaritons (SPs). The measured permittivity spectra were used to calculate the SP mode heights above the bismuth surface and SP propagation length, which satisfied our criteria for sensors.

A conducting polymer and its composite with graphite were also investigated since their plasma frequency may lie in the infrared region. Polyaniline was chemically synthesized and doped with various acids to prepare its salt form. A composite material of polyaniline with colloidal and nano-graphite was also prepared. Optical constants were measured in the long wave infrared region (LWIR) and were used to calculate SPP propagation length and penetration depth. SPP resonance spectra were calculated and suggested that polyaniline and its composite can be used as a host with sufficient mode confinement for IR sensor application.

Dedicated to my Parents

ACKNOWLEGDMENTS

I would like to thank my advisor Dr. Robert E. Peale for allowing me to work in his research group. I am truly grateful for his guidance and encouragement to complete this research project, and to become an independent researcher. I would also like to thank Dr. Helge Heinrich, Dr. Kevin Coffey and Dr. Diego Diaz for serving on my dissertation committee and taking their time reading and evaluating it.

I would like to acknowledge the help of Dr. Glenn Boreman and Guy Zummo for allowing me to use IR ellipsometry in their lab. I am also thankful to Dr. Diego Diaz and Dr. Yi Liao, for allowing me to work in their labs for chemical synthesis of conducting polymers. Thanks to David Bradford for all the machine shop work.

Dr. Walter Buchwald and Dr. Richard Soref deserve thanks for their contribution to this work and helping to edit my papers.

The majority of this research was funded by AFOSR and the Fulbright Fellowship, for which I am really thankful. I am also thankful to the Department of Physics for providing a teaching assistantship.

I would like to acknowledge my colleagues Dr. Justin Cleary, Dr. Gautam Medhi, Chris Fredricksen and Dr. Andrei Muravie for their direct contribution to this work. I thank all of my friends in our research group, Deep Panjwani, Janardan Nath, Farnood Rezaie, Nima Nader,

Pedro Figueiredo, Imen Rezada, Javanah Boroumand, Doug Maukonen, Dr. Tatiana Brusentsova, Evan Smith, Mehmet Yesiltas, and Jonathan Arnold. I am also thankful to Ted Gorman, Candace Alber, Valentine John and Rahul Hegishte for helping me prepare samples in their chemistry lab.

I am grateful to Dr. Talat Rahman and Dr. Richard Klemm for their guidance and support during my graduate school at UCF.

I wish to thank all the people whom I met during my graduate education who became my closest friends especially J. Christy Wilson III, Kevin Scott, Artsveni Nersisyan, Billy Campbell, Aubrey Truex, Pastor Charmaine Townsend, Tiffany and Kevis Brown, David and Becky Abraham, Dave Headberg, Pastor Phil Waisnen, Kimberly DeMars, Dr. Tom Cumming, Rebecca Walton, and my roommates Hari Paudel, Sartaj Singh Bhullar, Ali Maknounejad, and Iftikhar Jaim. I appreciate all the emotional and spiritual support from all of my friends throughout these years. I also acknowledge my parents Shahzad Pervaiz, Mrs. Rafia Shahzad, my siblings Neelam Shahzad, Suleman Shahzad, Karen Shahzad, Nouman Shahzad and my brother-in- law Imran Louis for all their support and encouragement.

Finally, I give thanks to God through Jesus Christ my Lord and Savior for all the good things that I have learned in the United States.

TABLE OF CONTENTS

LIST OF FIGURES

LIST OF TABLES

CHAPTER ONE: INTRODUCTION

Surface plasmons (SP) are electromagnetic surface modes coupled to longitudinal oscillation of surface charge density that propagate along a metal dielectric interface. These surface modes have attracted much scientific attention over the last one hundred years. Their excitation was first observed experimentally by Wood in 1902 [1] in the spectra of ruled diffraction gratings. He observed an uneven and unexpected distribution of dark and bright bands in the spectra of transverse magnetic (TM) light reflected from a grating. The theory of the diffraction grating was unable to explain the anomalies.

Lord Rayleigh (1907) [2] gave the first theoretical explanation of the bright anomalies in the (TM) spectra. The sharp change in reflectivity observed by Wood is generally referred to as the Rayleigh anomaly. He found that the scattered field is singular at wavelengths at which one of the diffracted order emerges from the grating at the grazing angle which results in a sudden redistribution of the available energy. Over the next three decades, these results were verified by Wood and other scientists.

Fano (1941) [3] connected the earlier theoretical work on radio waves propagating along the surface (Sommerfeld and Zenneck modes) of a conductor of finite conductivity to explain the experimental results of Wood and Rayleigh.

Pine and Bohm (1956) [4] gave the idea for treating electrons in a metal as plasma. Ritchie (1957) [5] coined the term "*plasmons"* for the plasma oscillation associated with quanta of collective excitation of free electrons in solids. It was confirmed by Ferrel (1958) [6] that the

density of oscillation of these electrons occurs in multiples of the quantum of energy $\hbar\omega_p$ where ω_p is the plasma resonance frequency. Hessel and Oliner (1965) [7] presented a new theoretical explanation of "Wood's anomalies," showing that there are two types of anomalies. They called them *Rayleigh* and *resonant* type anomalies. Later in (1968), Ritchie [8] experimentally showed that the guided wave anomalies found in metal reflection gratings were due to optically excited surface plasmons (known as surface plasmon polaritons), identified as the resonant type anomaly described by Hessel [7]. Otto [9] and Kretschmann-Raethers [10] (1968) used the phenomena of total internal reflection in a high index prism near a metal interface to excite SPP optically. SPP can also be excited electrically using electron beams. In this work grating couplers will be used.

Plasmonics has diverse applications, which range from biosensing, integrated circuits, solar cells, metamaterials, cancer biology and even art [11]. Most of these applications use noble metals (Au and Ag) as hosts for exciting surface plasmons in the visible or near IR wavelength regime. While noble metals provide the requisite negative electric permittivity for subwavelength confinement, they are also characterized by a significantly large imaginary component of the permittivity which causes loss in long-range plasmon propagation [12]. The field of plasmonics needs novel plasmonic materials which allow subwavelength optical confinement and loss mitigation at the same time [13, 14]. This provides motivation to study other materials, such as highly doped semiconductors, semi-metals and doped conducting polymers, as alternatives to noble metals.

Unlike noble metals, doped semiconductors provide greater flexibility to excite SPP because their plasma frequency can be tuned by doping, which makes them potentially attractive

for SPP spectroscopy for biosensing applications at IR frequencies [15-18]. Semimetals are also possible alternative plasmonics materials in the infrared range because their carrier concentration is 100 times less than that of noble metals [19]. Conjugated polymers in their undoped state are insulators, but they can be doped chemically via oxidation or reduction, which causes a transition from insulator to metallic/semiconductor state. They exhibit novel properties not typically available in metals and semiconductors. They have lower charge carrier density than noble metals and their plasma frequency is low such that $\hbar\omega_p < 1\ eV$; i.e., as high as mid to far infrared wavelength [20]. Therefore they offer a possibility as hosts for SPPs at mid-IR frequencies.

Table 1 summarizes optical properties of doped semiconductors, polymers and semimetals on the basis of their carrier concentrations and carrier mobility, which can be tuned and optimized for SPP resonances at IR frequencies. In plasmonics, high carrier concentration and carrier mobility are desired in order to provide a negative real part of the dielectric permittivity and low Drude damping losses, respectively [21].

Table 1: Optical properties of some novel materials.

Materials	Carrier Concentration (cm^{-3})	Carrier Mobility (cm^2/V-s)	Conductivity (S/cm)	Refs.
p-doped Silicon	10^{19} - 10^{22}	100-1000	10^{-4}- 10^{2}	16,24
Bismuth	$>10^{19}$	>1	10^{2}-10^{4}	24
Doped Polyaniline	~ 2 - 5 x 10^{21}	10^{-1}-10^{-2}	10-1000	59

Since many organic molecules have absorption resonances at IR frequencies, using non-metallic novel materials with mid-IR plasma frequencies as SPP hosts may increase the sensitivity of a surface plasmon resonance sensing system [22, 23]. This dissertation investigates infrared surface plasmon excitation in IR plasmonics materials.

The subsequent chapters of this dissertation are organized in the following manner:

Chapter 2: This chapter gives the physics and properties of SPP propagation on surfaces of various novel materials. The SPP dispersion relation and basic theoretical formulas for optically excited surface plasmons on gratings are presented. A modified Drude model for novel materials is discussed. Characterization methods for various SPP host materials and experimental techniques to measure surface plasmon resonance (SPR) are discussed.

Chapter 3: The study of the heavily doped semiconductor silicon as a host for infrared surface plasmons is presented here. Theory of Hessel and Oliner is presented here for calculation of SPR spectra and for later use in subsequent chapters. Experimental SPR reflectance measurements for Si gratings are compared with theoretical results using Hessel and Oliner theory. Figures of merit for tight mode confinement and plasmon propagation are also discussed.

Chapter 4: The study of the semimetal bismuth as a host for infrared surface plasmons is presented here. Ellipsometry data that differ strongly from previously published values are presented. Measurements of the excitation of electromagnetic surface modes (surface polaritons) are presented. Calculations of surface polaritons (SPs) propagation length and mode heights are discussed.

Chapters 5 and 6: IR optical constants of conductive polymers polyaniline and its composite polyaniline-graphite are investigated. Measured permittivities for these materials are used to calculate surface plasmon properties in the infrared region. Calculations predict their use in plasmonics applications.

Chapter 7: The work that has been completed in this dissertation is summarized, and possible future work is described.

CHAPTER TWO: MID INFRARED SURFACE PLASMONS ON NOVEL MATERIALS

2.1 Motivations

Surface plasmons represent coupling of an electromagnetic field to the kinetic motion of free charge carriers. A challenge facing plasmonics is propagation loss. Noble metals have a negative real part of their permittivity and fulfill the condition for subwavelength confinement at visible wavelengths. Novel materials, which may have tunable optical properties, may allow subwavelength confinement at IR wavelengths and hence are worth investigating [24]. Such materials with an engineered plasma frequency that extends the range of SPP applications to mid-infrared wavelengths may have unique sensing applications. Such considerations motivate our investigation of highly doped semiconductors, semimetals, and doped conducting polymers.

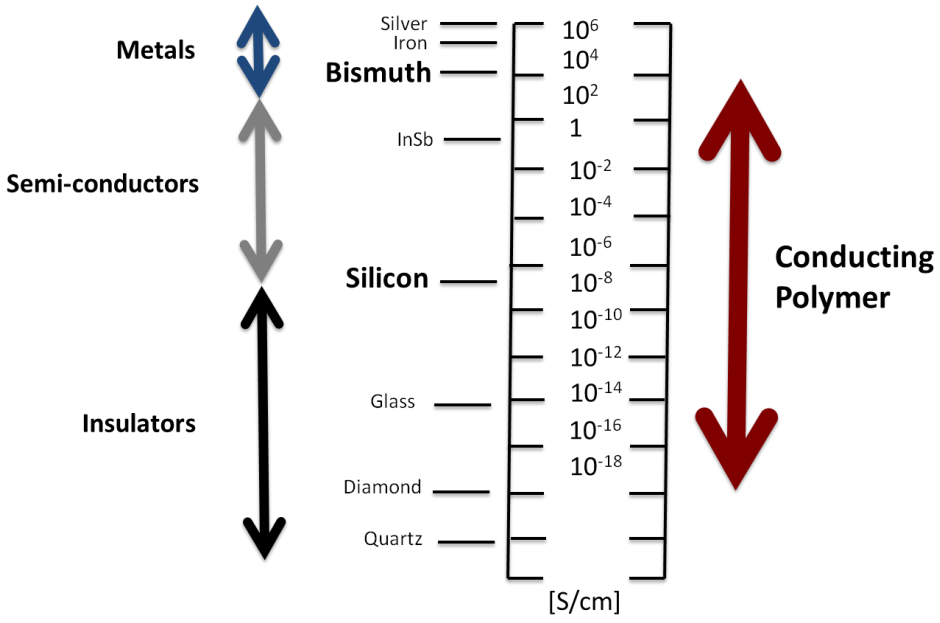

Figure 1: shows the electrical conductivities of the materials from insulators to metals [25].

2.2 Theory of Surface Plasmon Polaritons

Surface plasmons exist at the boundary between dielectric and conductor. Oscillation of surface charge density σ is the source of the electric fields. A discontinuity of the normal component of the exterior electric field at the boundary of dielectric and conductor with dielectric functions ε_d and ε_c, respectively, is given by [26],

$$E_{z1} - E_{z0} = 4\pi\sigma \quad , \tag{2.1}$$

where E_{z1} and E_{z0} are normal components of electric field in the conductor and dielectric respectively. The charge oscillations and electric fields above the surface are schematically shown in Figure 2. The wave function for a traveling charge density wave is:

$$\sigma(x,t) = \sigma_0 e^{i(K_x x - \omega t)} \quad . \tag{2.2}$$

Here K_x is the wave vector along the boundary. The charge oscillations are coupled with external electric field (E_x, E_z), which has components normal to the surface and in the propagation direction, and the transverse magnetic field (H).

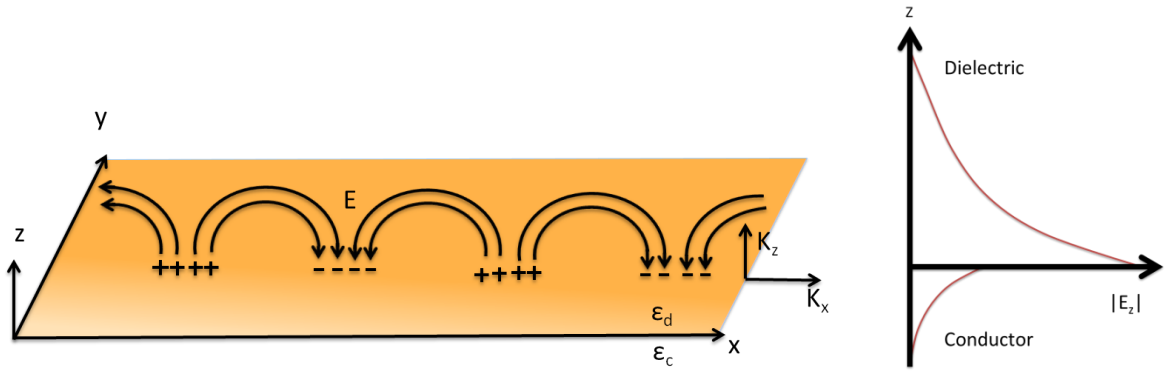

Figure 2: (left) Schematic of SPP electric fields and charge density. (right) Schematic showing exponential decay of fields into the dielectric and conductor [26].

The SPP is a p-polarized electromagnetic wave because its electric field vector **E** lies in the plane (x, z) defined by the surface normal and the propagation vector while the magnetic field vector **H** is perpendicular to this plane. The SPP electromagnetic field at the interface decays exponentially into both media as shown schematically in Fig. 2. The wave function for the normal component of the electric field is

$$E_z = \text{const}\, e^{i(K_x x + K_z z - \omega t)} \quad , \qquad (2.3)$$

where K_z is mostly imaginary. This causes exponential decay from interface, making SPPs evanescent waves. The energy density can exceed that of the incident radiation that excites the SPP. This high field energy confinement at the interface is one reason why SPPs are attractive for various applications [27]. The wave vectors K_x and K_z are related according to

$$K_x^2 + K_{zd,zc}^2 = \varepsilon_{d,c}(\omega/c)^2 \quad , \qquad (2.4)$$

where $\varepsilon_{d,c}$ is the complex dielectric function of the dielectric or conductor, respectively. We can obtain the complex wave vector of the plasmon in the z-direction

$$K_{zd,zc} = \sqrt{\varepsilon_{d,c}(\omega/c)^2 - K_x^2} \quad . \qquad (2.5)$$

If the imaginary part of $K_{zd,zc}$ is larger than the real part, then field penetration depth into the medium is less than the wavelength, and the SPP mode is non-radiative. Otherwise, it is considered to be radiative. SPPs of both types of modes travel along the interface with the complex wave vector K_x , which we will refer to as $K_{SPP.}$ The frequency, ω, and the wave vector of the SPPs are related by a dispersion relation $\omega(K_{SPP})$, which is different for radiative

and non radiative SPP modes. The dispersion relation for the non-radiative SPP mode can be derived by applying Maxwell's equations together with the continuity conditions for E and H [25]. For p-polarized oscillations ($E_y = 0$, $H_x = H_z = 0$), boundary conditions yield

$$\varepsilon_d K_{zc} + \varepsilon_c K_{zd} = 0. \tag{2.6}$$

Combining Eqs. (2.5) and (2.6) one obtains the surface plasmon wave vector K_{spp}

$$K_{SPP}(\omega) = (K_x' + iK_x'') = (\omega/c)\sqrt{\frac{\varepsilon_d \varepsilon_c}{\varepsilon_d + \varepsilon_c}} \tag{2.7}$$

Since the $\varepsilon_c(\omega)$ is complex, the K_{spp} in Eq. (2.7) consists of real (K_x') and imaginary(K_x'') parts, which describe propagation and damping, respectively.

According to the Drude model for metals, the electrons in a conductor behave like an ideal gas, and the real part of the dielectric constant for a conductor varies as

$$\varepsilon_c(\omega) = 1 - \frac{\omega_p^2}{\omega^2} \quad , \tag{2.8}$$

where the plasma frequency is

$$\omega_p^2 = \frac{Ne^2}{m\varepsilon_o} \quad , \tag{2.9}$$

where N is free electron density, m and e, the mass and charge of electron, and ε_o the permittivity of free space. Substituting the dielectric function of the conductor into the dispersion relation of Eq. (2.7) and solving it for K_x as a function of ω yields two solutions. The one with positive root leads to unbound modes whose dispersion curve is asymptotic to the light line $\left(\omega = cK_x/\sqrt{\varepsilon_d}\right)$ at high frequency. The negative solution leads to bound or SPP modes. These modes approach the

light line asymptotically at a low frequency $\omega << \omega_{p.}$ For large K_x, this branch saturates at $\left(\omega_p/\sqrt{1+\varepsilon_d}\right)$. In the case of ($\varepsilon_{air} = \varepsilon_d = 1$), the frequency of uncoupled dipole oscillation approaches $\omega = \left(\omega_p/\sqrt{2}\right)$.

SPP dispersion relation is schematically shown in Figure 3. It never crosses the light line. Therefore SPPs cannot be excited by simply irradiating a smooth conductor's surface because of the momentum mismatch between the surface plasmon and incident photon. Hence, additional methods are required for exciting SPP with incident electromagnetic radiation.

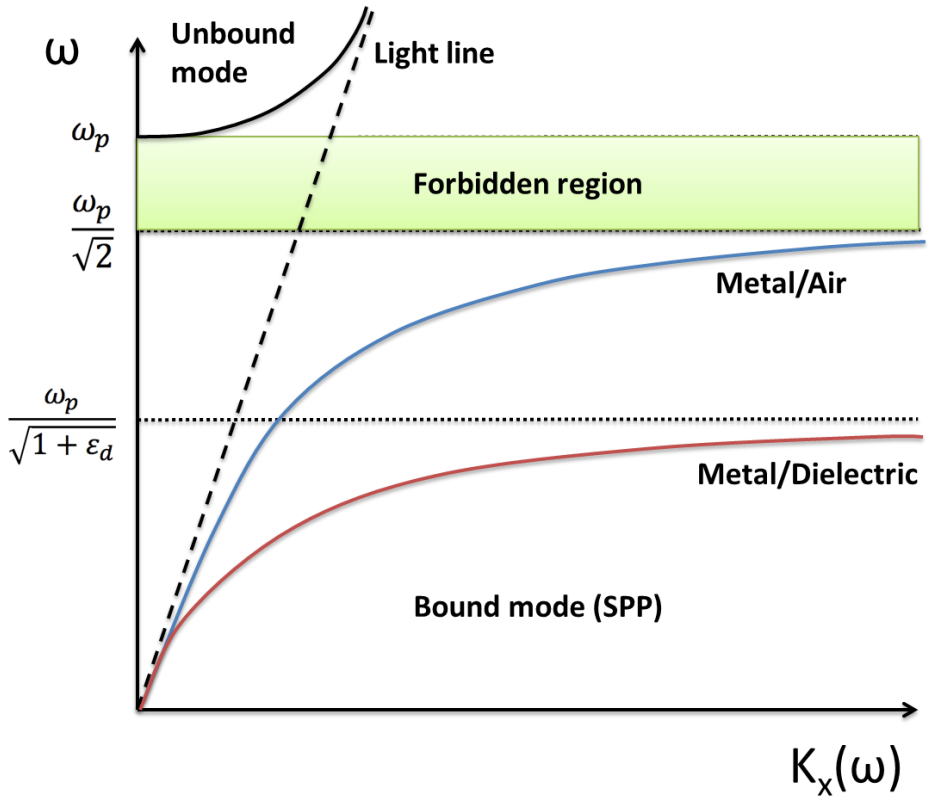

Figure 3: Dispersion relation for bound and unbound surface plasmons.

The field intensity of SPPs also decreases exponentially both in conductor and dielectric as $\left(e^{-|K_{zd,zc}||z|}\right)$. The values at which the field falls to 1/e, are given by

$$L_{d,c} = \left[\left(\frac{\omega}{c}\right) \mathrm{Re}\sqrt{\frac{-\varepsilon_{d,c}^2}{\varepsilon_d+\varepsilon_c}}\right]^{-1} \quad , \qquad (2.10)$$

The intensity of SPPs as they propagate along the surface decreases exponentially as $\left(e^{-2K_x''x}\right)$. The decay length, L_x, where the intensity has decreased to 1/e is given by

$$L_x = (2K_x'')^{-1} \quad . \qquad (2.11)$$

which we refer to as the SPP penetration depth. There are two methods of coupling light to SPPs, prism and grating coupling. We shall discuss the grating method first. If light hits a grating with a grating constant *a* at an angle Θ with respect to the normal of the plane, the component of its wave vector along the grating surface is increased or decreased by integer multiples of the grating wave vector $G = \left(2\pi/a\right)$. The grating structure may couple radiation to the SPP according to the coupling condition

$$K_{spp} = \sqrt{\varepsilon_d}K_o\sin(\theta) \pm nG \text{ , } n = 0, \pm1, \pm2, \pm3,\ldots \qquad (2.12)$$

Figure 4 illustrates schematically the coupling by a grating. Positive and negative values for K_{spp} are allowed corresponding to SPPs propagation in the same or the opposite direction as the in plane component of the incident wave vector.

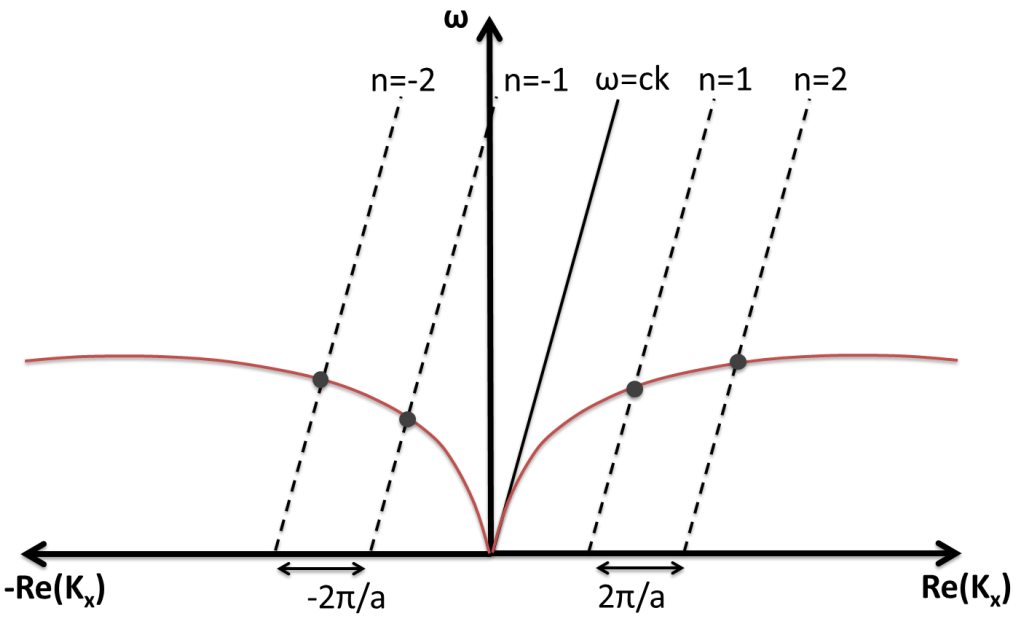

Figure 4: Schematic of grating coupled SPP for p-polarized incident radiation. The slope of the light line is csin(θ).

The line through the origin is the light line for a particular angle of incidence. The dashed lines parallel to the light line have been shifted by integer units of grating momentum. SPP dispersion curves are also shown which intersect the straight lines and define the possible IR frequencies where SPPs can be excited for the given angle of incidence. Alternatively, for a given frequency, as in our experiments, SPPs can be excited only at specific angles of incidence.

Prism couplers (hemicylindrical and triangular prisms) are also known, but these are difficult to use at IR frequencies. In the case of a hemicylindrical prism, the high refractive index of the IR prism material forms a high Q cavity with Fabry–Perot resonance artifacts obscuring the resonance spectra which can be reduced using a triangular prism. But the triangular prism gives non-linear relation between the angles within and outside the prism and a limited range of incidence angles [28]. Therefore in this work, gratings were used as IR SPP

couplers. These were formed by photolithography, reactive ion etching (RIE), and metal evaporation.

2.3 General Characterization Methods for SPP Host

Various materials were characterized for studying surface plasmon hosts using gratings or thin films deposited onto gratings for plasmon excitations. The methods of their synthesis and specific characterization techniques of surface plasmon hosts will be discussed in their respective sections.

Infrared transmittance spectra of deposited films of the semimetal bismuth, a conducting polymer polyaniline, and its composite polyaniline-graphite, were collected using a BOMEM DA8 Fourier transform spectrometer. Resources were a Globar or mercury lamp source, a 4K Bolometer, HgCdTe or DTGS detector, and Mylar or KBr beam splitters. A silicon wafer substrate polished on both sides was used for reference transmittance measurements. The transmittance of a thin film is

$$T(\lambda) = s \exp[-2d/\delta(\lambda)] \quad , \qquad (2.13)$$

where d is the film thickness, δ the 1/e decay length of the electric field into the conductor, λ the wavelength, and *s* is a constant that depends on surface reflectance and scattering.

The transmittance measurement allows the determination of infrared penetration depth of the film. This is needed since we need optically thick films for subsequent IR ellipsometry measurements. The transmittance for two samples of same material with different film thicknesses determines δ according to

$$\delta = \frac{2(d_2 - d_1)}{\ln\{T_1(\lambda)/T_2(\lambda)\}} \tag{2.14}$$

A second method to determine the infrared penetration depth is by calculating it from empirical permittivity data, according to

$$\delta = {}^{c}/_{\omega}\, Im\left(\sqrt{\varepsilon_c}\right). \tag{2.15}$$

Complex permittivity spectra were measured using a J. A. Woollam IR-VASE ellipsometer for doped silicon, bismuth, polyaniline, and its composite material. The raw ellipsometry output data ψ and Δ were measured for three angles of incidence (60, 65, and 70) and calculated complex permittivities averaged, where ψ and Δ are the complex reflectance ratio of p-polarized light to s-polarized light and the phase shift between the two complex reflectances, respectively [29].

The real and imaginary parts of the complex permittivity, for a given angle of incidence Θ, are

$$\varepsilon' = \sin^2(\theta)\left[1 + \frac{\tan^2(\theta)\left(\cos^2(2\Psi) - \sin^2(\Delta)\sin^2(2\Psi)\right)}{(1+\sin(2\Psi)\cos(\Delta))^2}\right], \tag{2.16}$$

$$\varepsilon'' = \sin^2(\theta)\left[1 + \frac{\sin^2(\theta)\tan^2(\theta)\sin(4\Psi)\sin(\Delta)}{(1+\sin(2\Psi)\cos(\Delta))^2}\right]. \tag{2.17}$$

The refractive index n and excitation coefficient k can be found from complex permittivities by

$$\varepsilon' = n^2 - k^2, \tag{2.18}$$

$$\varepsilon'' = 2ink. \tag{2.19}$$

A modified Drude model has been fit to the permittivity spectra,

$$\varepsilon(\omega) = \varepsilon_\infty \left(1 - \frac{\omega_p^2}{\omega^2 + i\omega\gamma}\right) \tag{2.20}$$

where γ is the relaxation time of the free electrons [30]. The high frequency limit of the permittivity is given by $\lim_{\omega\to\infty} = \varepsilon_\infty$, and accounts for the background polarizability of the bound electrons in the undoped semiconductors. The background polarization affects the plasma frequency given by

$$\omega_p^2 = {Ne^2}/{(\varepsilon_\infty \varepsilon_o m^*)} \tag{2.21}$$

Since the doping concentration N in the conductors studied here is several orders of magnitude lower than the free carrier concentration in noble metals, the plasma frequencies of these materials are much lower, in the infrared region [31]. The value of high frequency permittivity for the investigated materials lies in the range $1 < \varepsilon_\infty < 100$, [19], unlike noble metals where free carrier effects are dominant so that $\varepsilon_\infty = 1$ has the value unity.

The experimentally determined complex dielectric functions are compared with the modified Drude model Eq. (2.20), to obtain values for the relaxation and plasma frequencies of the materials investigated. The resistivities of our films were measured via a four point probe method. Values were compared with resistivities calculated from the Drude model based on optical constants, according to [32]

$$\rho = (\varepsilon'' \varepsilon_\infty \varepsilon_o \omega)^{-1} \quad . \tag{2.22}$$

Raman spectra were collected for elemental identification of samples of conducting polymers and their composites using a Renishaw RM 1000B Micro-Raman Spectrometer.

2.4 Experimental Techniques for SPR Reflectance Spectra

Surface plasmons were excited on gratings of different materials. These were mounted and aligned on a motorized goniometer. Specular reflectance as a function of the incidence angle was measured for the gratings using a quantum cascade laser (QCL) or IR LED and 77 K HgCdTe detector, or using a line-tunable CO_2 laser and power meter. In all cases, the laser radiation was p-polarized. The samples and detector were mounted on the θ and 2θ stages of the motorized goniometer, respectively. SPP generation was observed and measured as resonant decrease in the reflected intensity at certain angles. Data were recorded using a Labview program. The signal to noise ratio was increased using a boxcar averager or lock in amplifier. Experimentally measured SPR spectra were compared with calculations using the Hessel and Oliner theory [7]. Figure 5 presents a photograph of the experimental setup for measuring specular reflection spectra.

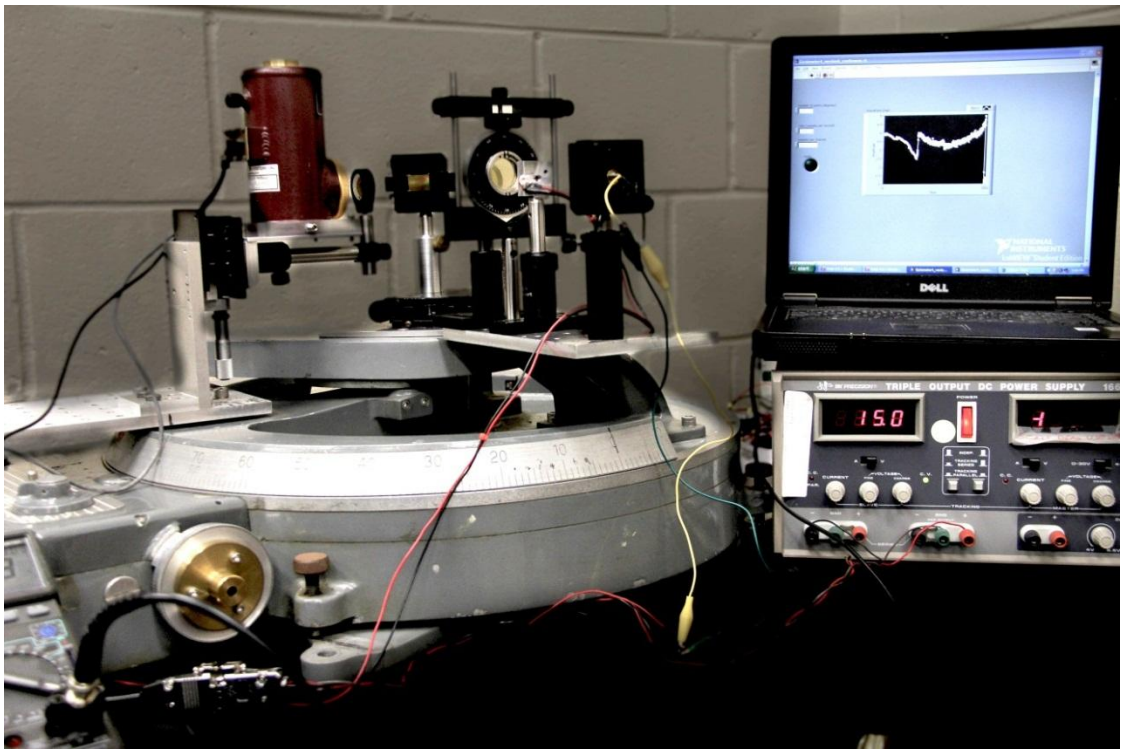

Figure 5: shows a picture of the experimental setup for measuring surface plasmon resonances using grating coupler. The base is a motorized goniometer, and on top is the IR radiation source QCL/IR LED the with HgCdTe detector. Specular reflection data were recorded using a Labview program on a laptop computer (right side).

CHAPTER THREE: INFRARED SURFACE PLASMONS ON HEAVILY DOPED SILICON

3.1 Introduction

Bound electromagnetic waves that propagate along the interface between a dielectric and a conductor exist below the plasma frequency of the conducting material when the real part of the permittivity ε' is negative [33]. Tight confinement of SPP energy to distances above the interface less than the corresponding free-space wavelength requires frequencies not too far below the plasma frequency, which holds at optical wavelengths for metals like gold and silver.

The principal existing application of SPPs is in biosensors where the change in the resonant coupling of light to SPPs indicates the binding of biomolecules to the conductor surface [34]. Commercial Surface Plasmon Resonance (SPR) biosensors work at visible or near infrared frequencies [35, 36]. It has been proposed that operating SPR biosensors in the mid-IR region may yield increased sensitivity and selectivity because the biological analytes are then differentiated by their IR fingerprint absorption spectra, and analyte refractive index changes are enhanced by the associated dispersion [28]. The long wavelength limit of one of the few previous IR SPR biosensor investigations [35] was 2.3 μm, which falls short of the range of characteristic molecular absorption lines. It has also been suggested [37] that these longer wavelengths are less likely to cause photo-induced damage to biological specimens, but the longest wavelength studied in Ref. [37] was 2 μm, well short of the molecular fingerprint region. In contrast, the experimental SPR results we present in this work are at 10 μm wavelengths.

Optimal overlap and interaction between IR SPPs and surface-bound analytes requires conductors with IR plasma frequencies [38]. One possibility is heavily doped silicon, whose long wave electrodynamic properties at carrier concentrations above 6×10^{19} cm^{-3} are those of a conductor that can support SPPs [38 - 44]. Doped Si as a mid-IR SPP host for SPR biosensors was suggested independently by Cleary *et al.* [38] and by Chen *et al.* [42]. The latter theoretically studied SPR on silicon gratings. A modified Si-based design was proposed and studied theoretically by DiPippo *et al.* [43]. Recently, Ginn *et al.* [15] experimentally determined the optical constants for a range of ion-implanted silicon samples and predicted their long-wave IR SPP properties. They wrote "The direct measurement of surface plasmon propagation can be experimentally quantified using standard prism coupling and grating scattering techniques." Preliminary experiments of SPPs on doped silicon by prism coupling [28] and grating scattering [44] has already been presented in conference proceedings. This paper presents a more extended experimental investigation of heavily doped silicon as an IR SPP host material and reports measured SPR effects on Si gratings.

Silicon is also interesting for p^+-Si/Si hybrid plasmonic and photonic waveguiding applications [39] which could allow for the integration of multiple functions on a single chip fabricated using standard silicon processing. Narrow subwavelength guiding regions of any desired shape and doping density are readily created by ion implantation through a photolithographic mask. SPPs are localized near the conductive, doped surface, which would act as a useful interface for analytes in advanced chem-bio plasmonic sensing architectures. SPPs, excited by photons at the doped-waveguide input and sensed via photonic coupling at the output could be utilized for spectrometer-on-a-chip applications. For example, Si plasmo-photonic

waveguide coupling may be achieved via two Si strip channel photonic waveguides on a silicon-on-insulator (SOI) substrate that are each coupled via a silicon taper to a doped-Si on Si plasmonic waveguide whose cross section is below the cutoff frequency at the operational wavelength. In addition to its photonic compatibility, the potential advantages of silicon plasmonics are its CMOS compatibility, its manufacturability in a foundry, and its ability to be biologically functionalized.

Small discrete plasmonic devices operate successfully in the near infrared and visible region. However, if we consider "elongated" devices that serve as plasmonic channel waveguides, then the SPP propagation loss becomes a figure of merit. A useful criterion is that the characteristic propagation length for SPP intensity should be at least twice the free-space wavelength [39]. This consideration favors long IR wavelengths, because the loss drops rapidly as the frequency is decreased below the plasma frequency ω_p. On the other hand, for biosensor applications, the mode should strongly overlap the surface bound analyte and hence should be tightly confined to the surface. A reasonable criterion is that the characteristic penetration depth for the electric field into the space above the conductor should be less than the free space wavelength [39]. However, the SPP mode height is sub-wavelength only near ω_p, and it increases rapidly for longer wavelengths. Thus, these two figures of merit with conflicting spectral requirements must be balanced and optimized.

The IR photonic/plasmonic waveguide suggested for illustration is a composite of conductors (doped Si) and dielectrics (undoped Si). The plasma frequency ω_p of the conducting regions is determined by the carrier concentration and carrier effective mass. In the undoped

regions, the material should be transparent, which is generally satisfied in the IR for semiconductors.

While the preceding discussion presents a vision for a silicon biosensor on micron length scales, actual commercial biosensors couple light to SPPs by illuminating a thin conducting layer through a bulk prism. The prism allows matching of photon and SPP momenta so that coupling can occur at the appropriate angle of incidence. Successful coupling is observed as a resonant decrease in the specularly reflected power. Infrared materials, and in particular Si, have high refractive indices which lead to strong interference artifacts in the angular reflection spectrum associated with hemicylindrical prisms and to impractically large apex angles for triangular prisms [28]. These problems associated with SPR biosensors at IR wavelengths motivates the alternative to prism couplers, namely grating couplers [42 - 45], which is the approach adopted in this experimental study of SPR excitations on doped silicon.

3.2 Theoretical Considerations

IR-to-SPP grating couplers function by adding positive and negative integer multiples m of $2\pi/p$ to the in-plane component of the photon wave vector, where p is the grating period [7, 26, 45]. This compensates for the inherent photon/SPP momentum mismatch. Grating couplers allow multiple SPP excitation resonances due to multiple units of grating momentum that may be added, if higher harmonics of the grating period occur in its profile [45]. The coupling condition between an IR wave, which is incident from a dielectric at an angle θ onto a conducting grating of period p, and an SPP is

$$\eta_d \sin(\theta) + m\frac{\lambda}{p} = \pm\frac{c}{\omega}\mathrm{Re}\left[k_{spp}\right] \qquad (3.1)$$

The refractive index η_d of the dielectric above the grating is important in biosensing applications, since it changes when analyte molecules bind to the surface and shift the resonance angles. In Eq. (3.1), the complex SPP wave vector k_{spp} is given by Eq. (2.7) [26], where c is the light speed, ε_d and ε_c the complex permittivity of dielectric and conductor, respectively, and ω the angular frequency. The complex permittivity spectrum $\varepsilon_c(\omega) = \varepsilon_c'(\omega) + i\,\varepsilon_c''(\omega)$ was determined from the measured IR ellipsometry spectra of our p-Si wafers using standard Fresnel Eqs (2.16) and (2.17), [29] and values at our laser wavelengths are presented in Table 2. For the measurements presented here, $\varepsilon_d = \eta_d = 1$, and the subscript 'c' in the conductor permittivity will be dropped in the subsequent discussion.

Calculation of angular reflection spectra was performed by using the theory of Hessel and Oliner [7, 26, 45]. This theory allows analytic calculation of the line shapes for absorption resonances that are associated with the generation of "guided complex waves supportable by the grating". Though the words "surface plasmon polaritons" do not appear in this early paper [38], the wave function and complex wave vector of the guided waves are identical to those of SPPs, so they are the same thing. Moreover, propagating SPPs associated with measured resonances that agree with such calculations have been directly observed [45].

We assume a simplified model of the grating as a sinusoidally modulated surface impedance, represented by

$$Z(x) = Z_o\left(1 + M\cos\left[\frac{2\pi x}{p}\right]\right). \qquad (3.2)$$

where *x* is the coordinate in the plane of the grating and perpendicular to the grooves, and *M* is a modulation parameter that is a function of grating permittivity, amplitude, and wavelength. This approximation neglects the higher Fourier components of the actual rectangular grating profile. Z_0, the average surface impedance, or the impedance in case of zero modulation is

$$Z_o = \sqrt{\frac{\mu_o}{(\varepsilon' + i\varepsilon'')\varepsilon_o}} = \frac{337\Omega}{\sqrt{(\varepsilon' + i\varepsilon'')}} \quad , \tag{3.3}$$

where μ_0, ε_0, and 377 Ω are, respectively, the permeability, permittivity, and impedance of free space. The average surface impedance relative to free space is

$$\xi = \frac{z_o}{377\Omega} = \frac{1}{\sqrt{\varepsilon' + i\varepsilon''}} \quad , \tag{3.4}$$

or

$$\xi = \begin{bmatrix} -i \\ 1 \end{bmatrix} (\varepsilon' + i\varepsilon'') \left\{ \cos\left(\frac{\varphi}{2}\right) + i\sin\left(\frac{\varphi}{2}\right) \right\} \; for \; \begin{pmatrix} \varepsilon' < 0 \\ \varepsilon'' > 0 \end{pmatrix} \quad , \tag{3.5}$$

where

$$\varphi = \tan^{-1}\left(\varepsilon''/\varepsilon'\right)$$

The experimentally determined permittivity values for heavily p-type doped silicon are given in Table 2, together with relative surface impedance values from Eq. (3.5).

Table 2: Optical parameters of heavily doped p-type silicon.

N($\times 10^{19}$cm^{-3})	**λ(μm)**	**ε′**	**ε″**	**ξ[Eq.3.4]**
10	9.25	-11.4139	15.6130	0.1029-*i*0.2028
6	9.38	2.76364	4.80317	0.3677-*i*0.2126
10	10.59	-16.1949	20.9584	0.0856-*i*0.1744

Eq. (3.5) has four mathematically possible pre-factors (± 1, ± i) [46]. On physical grounds [32], we require $\xi' > 0$ and $\xi'' < 0$, which leads to just two pre-factors being retained, with each pertaining to particular permittivity conditions as shown in Eq. (3.6). The specular reflectance of the grating is calculated to good approximation by

$$R \approx \left| 1 - \frac{4\cos\theta}{M\xi\left(D_o - D_1^{-1} - D_{-1}^{-1}\right)} \right|^2 \quad , \qquad (3.6)$$

with D_n, defined as

$$D_n = \frac{2}{M}\left[1 + \frac{1}{\xi}\sqrt{1 - \left(\sin\theta + \frac{n\lambda}{p\eta_d}\right)^2}\right] \quad , \qquad (3.7)$$

with n an integer. The sinusoidal surface impedance approximation and the neglect of D_n terms with $|n| > 1$ in the formula for R give calculated angular reflectance spectra in which only the $m = 1$ resonance appears. Inclusion of higher order D_n terms in the formula for R has negligible effect on the reflectance spectrum in the angular regions accessible to our experiments. For fitting the measured angular reflectance spectra, M is the only parameter varied.

3.3 Experimental Considerations for Si Gratings

Commercial doped p-Si wafers with resistivities ρ = 0.0006 - 0.001 and 0.0018-0.0032 Ohm-cm were procured. These were boron-doped during the melt with uniform doping throughout the wafers. Resistivity values were confirmed by standard 4-pt probe measurements, and the carrier concentrations corresponding to our measured values for the samples studied are 1×10^{20} cm^{-3} and 6×10^{19} cm^{-3}, respectively [47]. Complex permittivity spectra of the unprocessed wafers were determined in the wavelength range 1 to 40 μm. Lamellar surface-corrugation gratings of 20 μm period, nominal 50% duty cycle, and various amplitudes (i.e. etch depth) were formed by standard photolithography and reactive ion etching. Profiles were confirmed using a step profilometer as shown in Figure 6.

Figure 7 presents a schematic diagram of the experimental setup for measuring the infrared specular reflection as a function of angle, where 'L', 'D', 'G' and 'GR' in diagram represent laser, detector, goniometer and grating. A p-polarized line-tunable CO_2 laser or quantum-cascade laser were used together with a laser power meter or a HgCdTe photodetector operated at 77 K, respectively. Dips in the reflected power at certain angles of incidence indicate the excitation of SPPs [26].

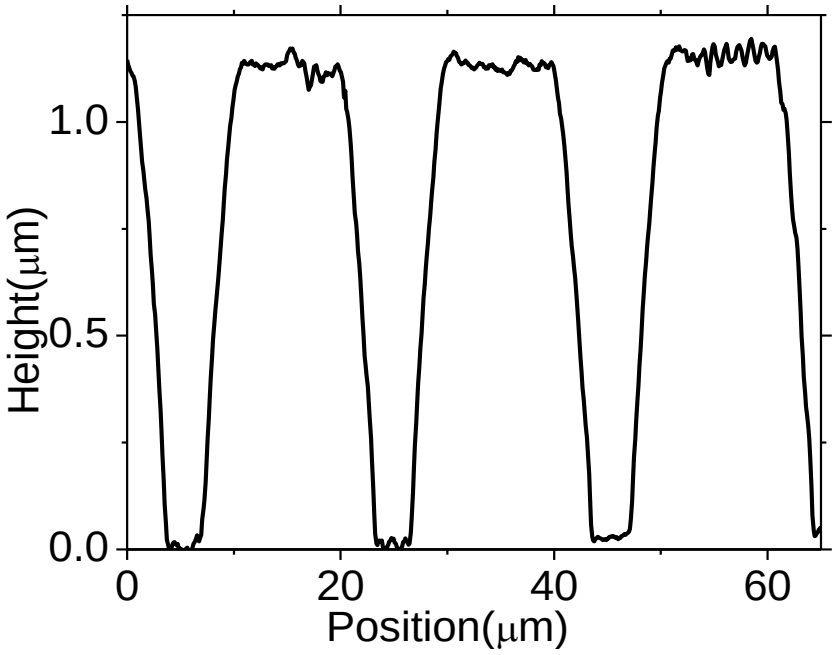

Figure 6: Doped Silicon lamellar grating profile for grating with h = 1.12 μm.

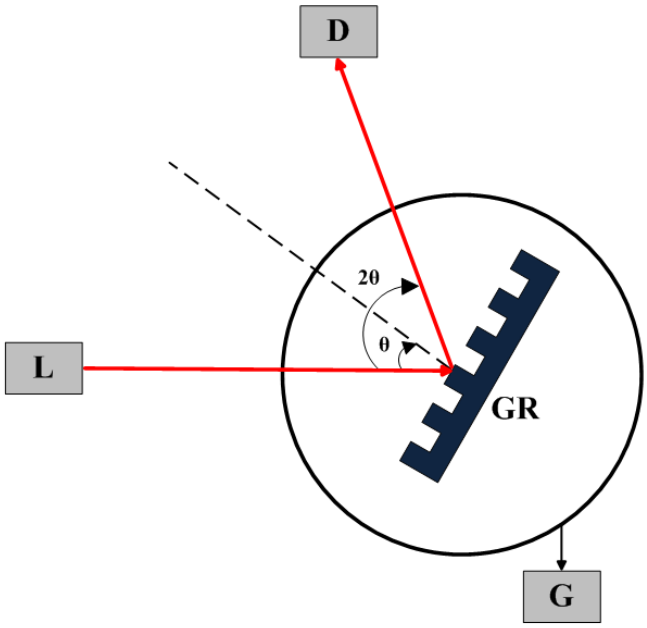

Figure 7: Schematic diagram of experimental setup for measuring the infrared specular reflection as a function of angle, where labels L, D, G and GR in diagram represent laser, detector, goniometer, and grating.

3.4 Results

Figure 8 presents permittivity spectra for both wafers. For the most heavily doped silicon, the ε' values are negative below 0.212 eV (wavelength $\lambda > 5.84$ μm). The imaginary part exceeds the magnitude of the real part, which is generally disadvantageous for SPP applications as ε'' is responsible for loss and SPR broadening. For the more lightly doped silicon, the ε' values are negative below 0.107 eV ($\lambda > 11.6$ μm). Here also ε'' exceeds the magnitude of ε'. At short wavelengths the real part of the permittivity for both materials approaches 11.3, which is close to the static dielectric constant value of 11.7, while the imaginary parts approach zero. The permittivity values for the doped p-Si, relevant to the experiments performed using CO_2 and quantum-cascade lasers, are given in Table 2, together with the relative surface impedance.

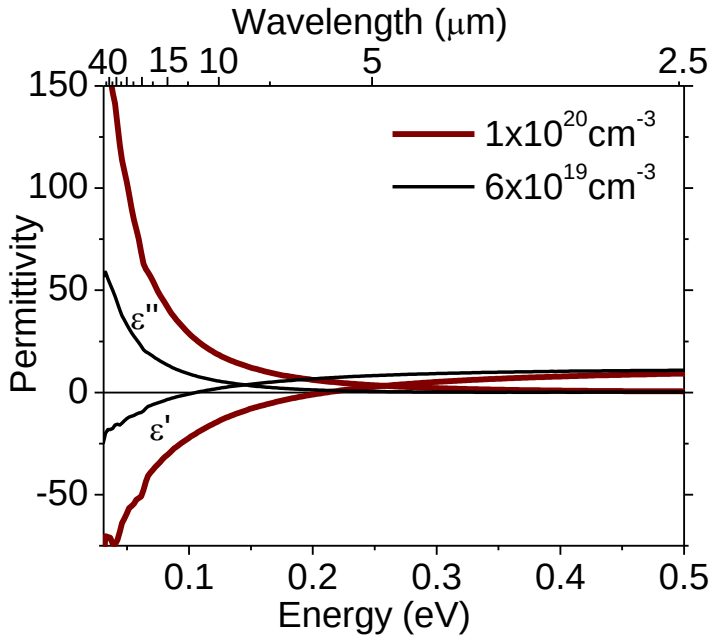

Figure 8: Real and imaginary parts of the permittivity for heavily-doped p-type silicon of different carrier concentration, as indicated in the legend.

Figure 9 presents the experimental reflected intensity as a function of angle of incidence at two different CO_2 laser wavelengths for gratings of different amplitude *h* made from the 1 x 10^{20} cm^{-3} silicon. The data have been normalized, so that the maximum experimental reflected power has the value unity, and the curves for increasing *h* have been offset vertically from each other by unity for clarity. For *h* = 0.45 μm, absorption resonances are just discernable for the 10.59 μm wavelength, while at 9.25 μm wavelength they are partly obscured by baseline noise fluctuations caused by the measuring system. In general, the resonances strengthen up to about *h* = 1 μm, for both wavelengths, after which broadening becomes severe for m = 1 case. For the m = -3 case, the resonance appears to increase in magnitude up to the largest h gratings studied. The resonances are rather broad for all grating amplitudes, as was anticipated from the large ε''

values. The m = 1 resonance, according to Eq. (3.1), occurs at 34.45 and 29.60 degrees for λ = 9.250 and 10.591 μm, respectively. These angles are indicated by symbols and the labels "1" in Figure 9. The m = -3 resonance occurs at 21.53 and 34.40 degrees for the two respective wavelengths. These angles are indicated by symbols labeled as "-3" in Figure 9. Angles from Eq. (3.1) are in good agreement with the observed reflectivity dips. Calculated resonance spectra are also plotted in Figure 9 as heavy black lines for h = 1.12 μm, where the best match was found using M = 1 in Eqs. (3.6) & (3.7). These calculated spectra closely resemble the experimental ones, except that as mentioned above, only the m = 1 resonance appears in the calculated curve because of the assumed sinusoidal impedance modulation with no higher harmonics.

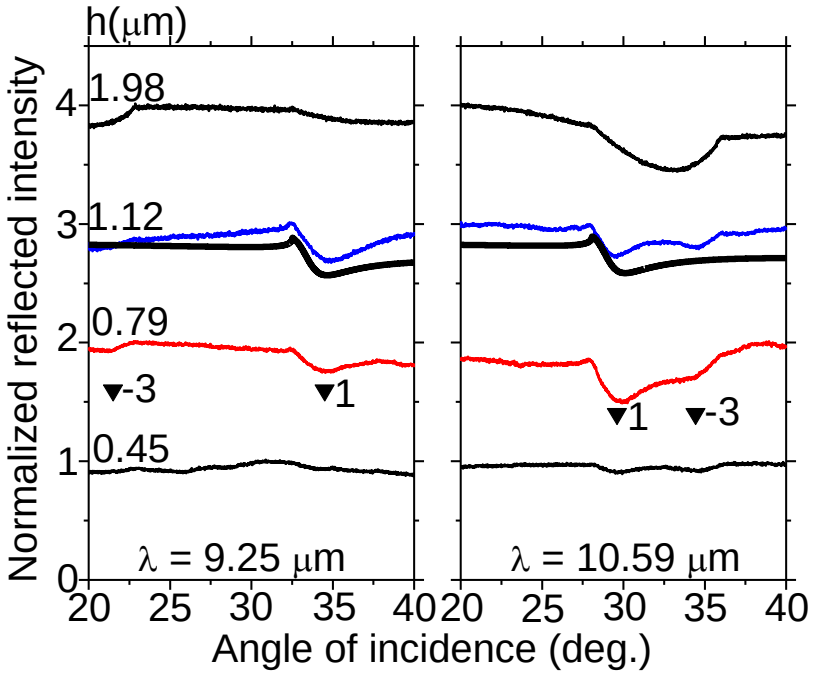

Figure 9: Experimental angular reflectance spectra for p-Si with carrier concentration of 1 × 10^20 cm^-3 fabricated into lamellar gratings of 20 μm period and with various amplitudes h as indicated. The heavy black curves for h = 1.12 μm are calculated spectra.

Figure 10 presents the experimental reflected intensity (thin curve, normalized) as a function of angle of incidence at the QCL wavelength of 9.38 μm for the silicon gratings of carrier concentration 6×10^{19} cm^{-3} and amplitude h = 1 μm. Only a baseline drift without suggestion of a resonance is observed. The cusp at ~34 deg. in the calculated resonance spectrum (heavy curve, un-normalized) with M = 1 in Eq. (3.7) suggests a hint of a resonance. The absence of a clear resonance excitation of an SPP is expected as no SPP should be supported at this wavelength for this material, since its permittivity is positive here (Table 2).

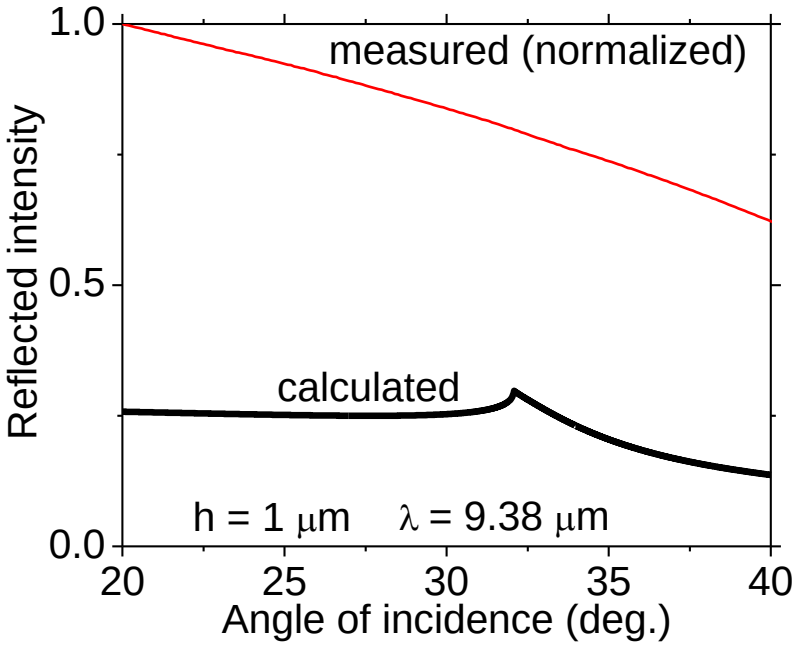

Figure 10: Experimental (thin curve, normalized) and calculated (heavy curve, un-normalized) angular reflectance spectrum at 9.38 μm wavelength excitation for the p+-Si with concentration 6 × 10^19 cm^-3. The lamellar grating had a 20 μm period with 1 μm amplitude.

Figure 11 presents the SPP field penetration depth L_d above the conductor surface calculated from Eq. (2.10) using the measured permittivity spectra. For carrier concentration 1×10^{20} cm^{-3} and $\lambda > 5.8$ μm, we have $\varepsilon' < 0$, so here this material supports a traditional bound SPP. For $\lambda < 5.8$ μm, $\varepsilon' > 0$ and ε'' approaches zero, so there the Si behaves like a dielectric: No bound SPP is supported and L_d quickly becomes >> λ. For carrier concentration 6×10^{19} cm^{-3}, the behavior is similar, but shifted to longer wavelength. Our criterion for application to a useful SPP-based sensor is $L_d < \lambda$. For carrier concentration 1 x 10^{20} cm^{-3} this holds for $5.1 < \lambda < 9.8$ μm. For carrier concentration 6 x 10^{19} cm^{-3}, it holds for $9.6 < \lambda < 16.6$ μm. By comparison, the sub wavelength confinement for doped silicon calculated by Ginn *et al.* [15] at p-type concentration of 10^{20} cm^{-3} occurs at somewhat longer wavelength, namely from 7 to 12 microns.

The difference is within the range of uncertainty for estimating the carrier concentration from the measured resistivity.

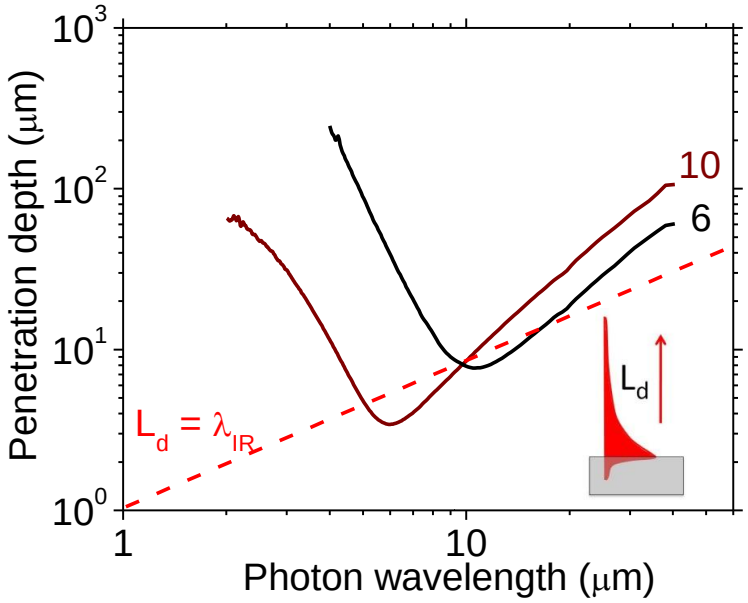

Figure 11: SPP field penetration depth into vacuum above the p+-Si surface. The part of the curves that fall below the dotted straight line (Ld = λ) are where the SPP electric field confinement is less than the free space wavelength. The numbers that label the curves give the carrier concentrations (x 10^19 cm^-3). The inset is a schematic to suggest the exponential decay of the SPP field away from the interface and the significance of Ld.

Figure 12 presents the characteristic SPP energy propagation length L_x as a function of free-space photon wavelength calculated from Eq. (2.11) using the measured permittivity spectra. Our criterion for adequate SPP propagation length [38], $L_x > 2\ \lambda$, holds for the long-wave parts of the curve that lie above the dashed line. The short-wave portions that lie above the dashed line apply to unbound EM waves, which nevertheless experience propagation loss due to interaction with the surface and thus have finite propagation lengths. For carrier concentrations 1×10^{20} and 6×10^{19} cm^{-3}, L_x exceeds 2λ for $\lambda > 6.05$ and 16.6 μm, respectively.

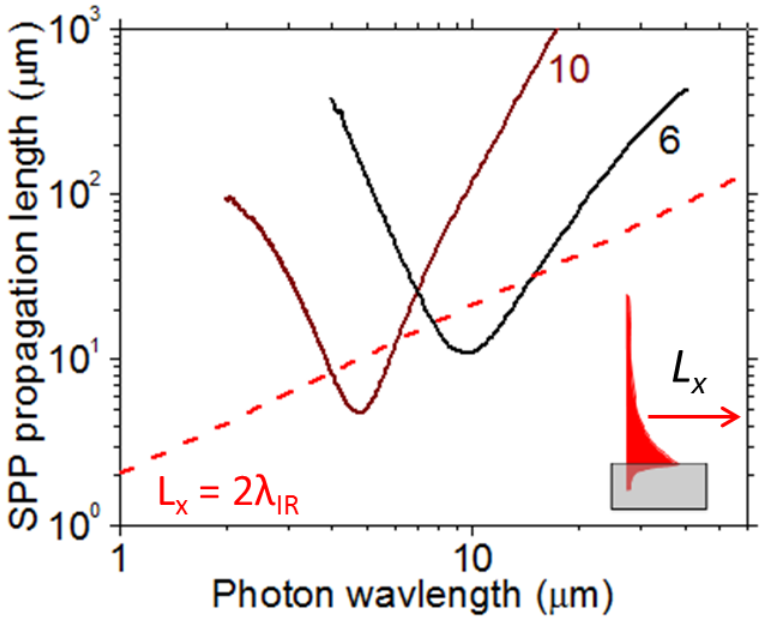

Figure 12: SPP energy propagation length versus free space wavelength. The regions with Lx > 2λ satisfies our criterion for the minimum useful propagation. The numbers that label the curves give the carrier concentrations (x 10^19 cm^-3). The inset is a schematic suggesting the exponential decay of SPP intensity away from the interface and the significance of Lx.

3.5 Discussion

Silicon plasmonic technology is a part of a more general plasmo-photonic technology in which plasmonic waveguides couple seamlessly to photonic waveguides, and vice versa, in order to give higher performance and/or new functionality. Silicon plasmonics is a part of the group-IV plasmonics approach wherein the composite plasmonic waveguides feature the semiconductors SiGe, Ge, or GeSn (as well as Si) together with the novel doped-Ge and germanicide conductors (as well as doped-Si and silicides [39]). The realm of group-IV plasmonics is largely uncharted as yet and is an excellent subject for future study. This chapter

presents, for this emerging field, some initial experimental results that are of particular relevance to potential IR sensor applications.

For Si plasmonics, conductors of doped poly-silicon [48], and doped strained silicon [49] are practical alternatives to doped crystalline Si. The strained versions are of particular interest due to enhanced mobilities. It is well known in the MOSFET industry that a layer of crystalline Si grown upon a relaxed layer of $Si_{0.7}Ge_{0.3}$ will result in a strained-Si layer whose electron and hole mobilities are increased by about 1.8 times. Higher mobility means longer relaxation time, lower loss for SPPs. The resulting smaller imaginary part of the permittivity would also give sharper SPP resonances than the ones observed here for bulk Si, leading to better biosensor sensitivity.

Calculated and experimental SPP resonances at 10 μm wavelengths were observed for p-Si lamellar gratings with a carrier concentration of 1×10^{20} cm^{-3}. The resonances were distinct, and although rather broad, they may have value for sensing applications. Adequate mode confinement and propagation lengths, according to our criteria for useful SPP-based sensing, were found for this material when the excitation wavelength is between about 6 and 10 μm.

For material with a carrier concentration of 6×10^{19} cm^{-3}, no SPP resonance was observed since the plasma wavelength is longer than our available laser wavelengths. Calculations based on measured permittivity spectra indicate that for this material there was no wavelength where the criteria for both mode confinement and propagation could be satisfied simultaneously.

CHAPTER FOUR: INFRARED SURFACE POLARITONS ON BISMUTH

4.1 Introduction

The semimetal bismuth (Bi) is one of those materials which have mid infrared plasmon frequency. Such materials are potentially useful hosts for infrared sensing based on surface plasmon polaritons (SPPs) resonance. In this paper we present the experimental and theoretical investigation of excitation of IR surface plasmon on Bi lamellar gratings in the wavelength range of 3.4 to 10.6 μm. Distinct SPP resonances were observed although the usual condition for bound SPP is not satisfied in this wavelength range. The excitation of these resonances agrees theoretically with the electromagnetic surface waves called surface polaritons (SPs) [50-52]. The measured infrared permittivity spectra of optically thick film of bismuth were used to calculate the SP mode heights above the bismuth surface and SP propagation length.

The electromagnetic SP wave propagates along the conductor surface. The field decays away from the surface. The usual condition for sustaining a surface plasmon is that the real part of the permittivity ε' be negative [26]. For typical metals such as Au and Ag, this condition holds for wavelengths in the visible and ultraviolet. The sign change for the permittivity occurs at the plasma frequency. However this condition for excitation of surface plasmon polariton (SPP) is not always required [19, 50-52]. Bound surface electromagnetic modes exist when the real part of the permittivity ε' is positive and smaller than the imaginary part of the permittivity ε''. Such electromagnetic modes are still surface polaritons (SPs), and the polarization that

serves as the source of the fields is still in the form of surface plasma waves, just as for the usual SPPs [53].

Infrared SPPs may have advantages in certain applications over SPPs at visible wavelengths. The plasma frequency of IR SPP hosts needs to be about one order of magnitude lower than that for typical metals, or equivalently, the carrier concentration needs to be about two orders of magnitude lower [12]. These conditions will allow tight mode confinement of the IR SP mode to the interface. Investigations of SPP properties for transition metals [38,56], doped silicon [15,16], the semimetal Sb [19], preliminary studies of the semimetals Bi and graphite, as well as the semiconductor CuSnS, have been published [28].

This work presents a more detailed determination of relevant IR SP properties for Bi, including the frequency-dependent propagation length, penetration depths for the fields into the media on either side of the interface, and first reports of SP excitation resonances. These values are calculated using optical constants that were measured over the wavelength range 1 to 40 μm. Plasma and carrier relaxation frequencies are determined from Drude-model fits to these data. Despite the usual criterion for bound SPPs, this work reveals distinct SPs generation resonances in the angular reflection spectra of Bi lamellar gratings at wavelengths where the real part of the complex permittivity is positive. This is possible due to the comparable magnitudes of the real and imaginary parts of the permittivity, such that there is little to distinguish between bound from unbound SPPs. The resonances reported here are potentially useful for IR sensor applications, which simply requires the existence of a suitable SP-photon coupling resonance that is sensitive to changes in the dielectric permittivity at the interface with the conductor.

4.2 Experimental Details

Bismuth films were thermally evaporated from 99.999% pure Bi pellets onto various substrates. The film thickness was monitored during evaporation using a crystal monitor. First, a thick film was deposited onto a glass slide and characterized using the IR ellipsometer in the wavelength range of 1 - 40 μm. The raw ellipsometer output was used to calculate the complex permittivity spectrum using standard Fresnel equations [29].

Lamellar gratings of 20 μm period, 50% duty cycle and different amplitudes were formed by photolithography and plasma etching in silicon. An optically thick Bi layer was then deposited on silicon gratings substrate which was characterized by using a Jeol SEM (scanning electron microscope), images of samples are presented in appendix A. The subsequent morphology of film was measured using a step profilometer. Specular reflectance as a function of incidence angle was obtained for the optically thick bismuth film on gratings using IR light emitting diode (LED) at 3.4 μm wavelength as well as with CO_2 and quantum cascade laser (QCL) at various IR wavelengths for non-optically thick Bi film. In all cases, the laser radiation was p-polarized i.e. with the electric field vector in the plane of incidence. The IR LED which was polarized using an infrared wire-grid polarizer, the grating samples and detector were mounted on the theta and 2-theta parts of a motorized goniometer, respectively. SPP generation was observed as a resonant decrease in the reflected intensity at certain angles [26].

4.3 Results

Figure 13 presents the real part of complex permittivity spectrum determined from ellipsometry (solid curves) for a Bi film of thickness 8 μm. This is compared with previously published results (symbols) for Bi. In Ref. [55], the Bi sample was formed by melting onto a piece of glass, then removed when it got solid while in Ref. [56], the sample was grown single crystal Bi in a furnace. These old results disagree considerably with our measured data. Our data shows that ε' crosses from positive to negative values at two different wavelengths 2.19 and 30 μm, as indicated by the vertical dashed lines in Figure 13. The crossing point for the data of Ref. [55] is at a slightly lower wavelength less than 2 microns. For Ref. [56] the real part of permittivity is always negative beyond 20 μm, and differs in sign from our measured data in the range 20-30 μm. Vertical line symbols indicate the laser and LED wavelengths used in our experiments.

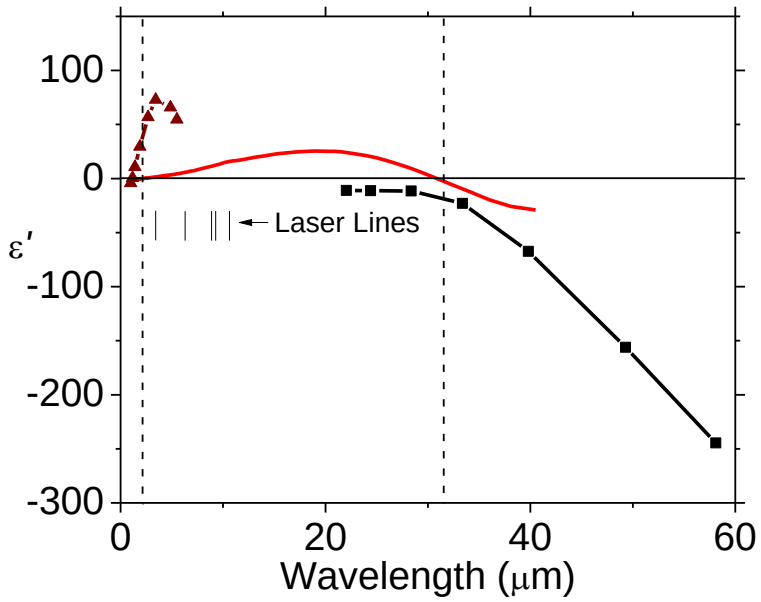

Figure 13: Real part of the permittivity for Bi evaporated film of thickness 8 micron. The triangle symbols are from reference [55]. The square symbols are from ref [56]. The smooth curve from the ellipsometry data of this work. The long dashed vertical Lines indicates the plasma frequencies.

Figure 14 shows the imaginary part of the permittivity of our measured data. Our data differ significantly from previously published results both in magnitude and slope, especially at the shorter wavelengths where we find Bi to be much less lossy than previously thought. Our ε'' values are at least double the magnitude of our ε' values at all the IR wavelengths we used to excite surface polaritons. This is in contrast to the usual condition for excitation of SPPs on ordinary metals at visible wavelengths where $|\varepsilon'| >> \varepsilon''$. They are comparable to each other at wavelengths less than 2.19 μm where $\varepsilon' < 0$.

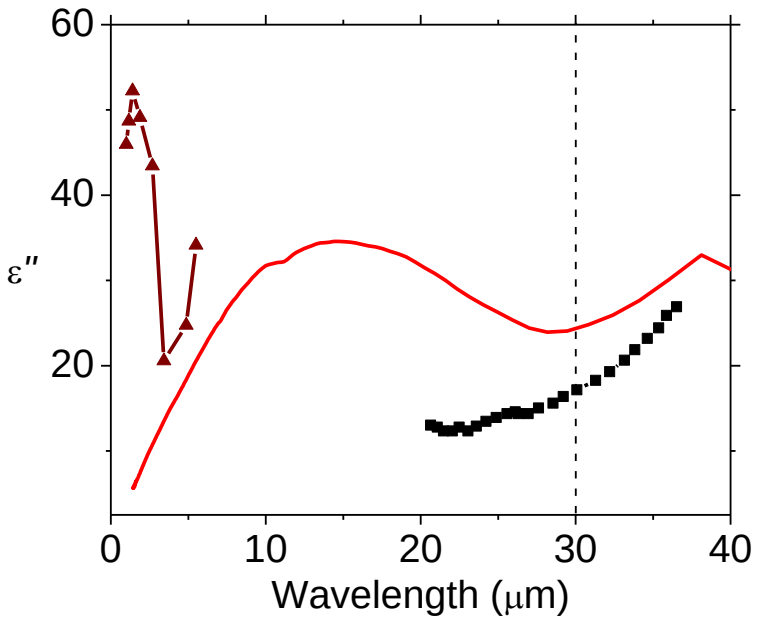

Figure 14: Imaginary part of permittivity for Bi. The triangle symbols are from ref. [55] and the square symbols are from [56]. The smooth curves are from the ellipsometry data of this work.

Transmittance spectra, T, of two Bi films having thickness d of 8.0 and 12 μm deposited on Si substrates, were measured. The IR penetration depth was found by Eq. (2.14), and was compared with the calculated values from the permittivity using Eq. (2.15). Near a wavelength of 10 μm, the maximum penetration depth is 5.4 microns.

Figure 15 shows the measured IR ellipsometry data for Bi films of various thicknesses. Fabry-Perot oscillations appear due to interference within the Bi film when the film thickness is less than the IR penetration depth. No oscillations were observed in measuring the complex permittivity data for a sample of Bi having film thickness at least 8 μm, which confirms the calculated and measured values of penetration depth. This also suggests that the way in which Bi samples are prepared has a significant effect on their optical properties.

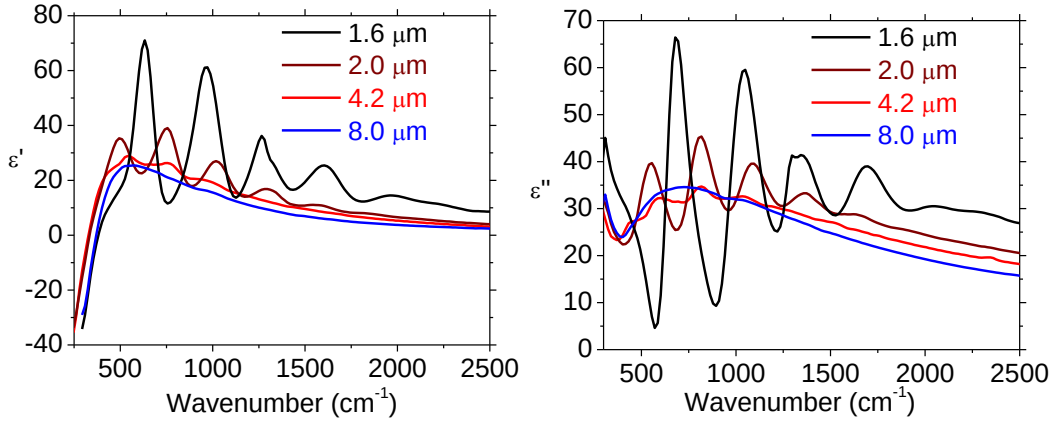

Figure 15: Thickness dependence of IR Optical constants of Bi films.

Drude constants were extracted by fitting modified the Drude model Eqs. (2.20) and (2.21) to the measured complex permittivity data of Figs. 13 and 14 for wavelengths in the range of 30 μm to 38 μm where the data is Drude like. The values obtained are ω_p = 0.04 eV, ω_τ = 0.009 eV, and $\varepsilon_\infty = 102 \pm 10$.

Figure 16 presents angular reflection spectra of Bi gratings using IR LED wavelength of 3.4 μm. The Bi film deposited was optically thick according to earlier penetration depth determination with thickness 6 μm. The values plotted are normalized reflected intensity. Resonances appear for grating amplitudes of at least 4 μm with grating period of 20 μm. The m = -2 resonance is calculated to occur at angle 25.4 deg. And for m = 1 resonance is expected to occur at angle of 36.8 deg. These positions are indicated by symbols. We expect the resonances to be broad because of the broadband nature infrared LED source. The expected uncertainty in the resonance positions is indicated by the horizontal error bar. The poor agreement for m =1,

the unexpected width of the absorptions, and a typical line shapes do not support the identification as SPP resonances at 3.14 μm.

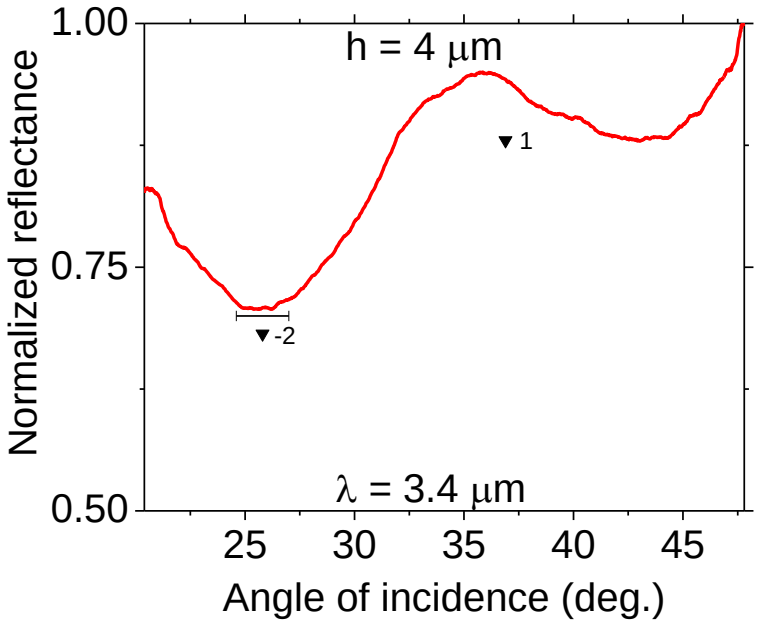

Figure 16: Angular reflectance spectra of Bi gratings at IR (LED) wavelength.

Figure 17 presents angular reflection spectra of Bi gratings using two QCLS and two laser wavelengths. In this case, deposited Bi film was not optically having thickness only 1.7 μm on Si substrate. The varying reflected intensity curves have been shifted vertically for clarity in the Figure 17. SP resonances this time appear clearly for various grating amplitudes. Since the uncoated Si gratings do not show any resonances [16], the observed resonances are due to the excitation of bound SPs on bismuth. What effective permittivity to use for the optically thin coating is still unclear.

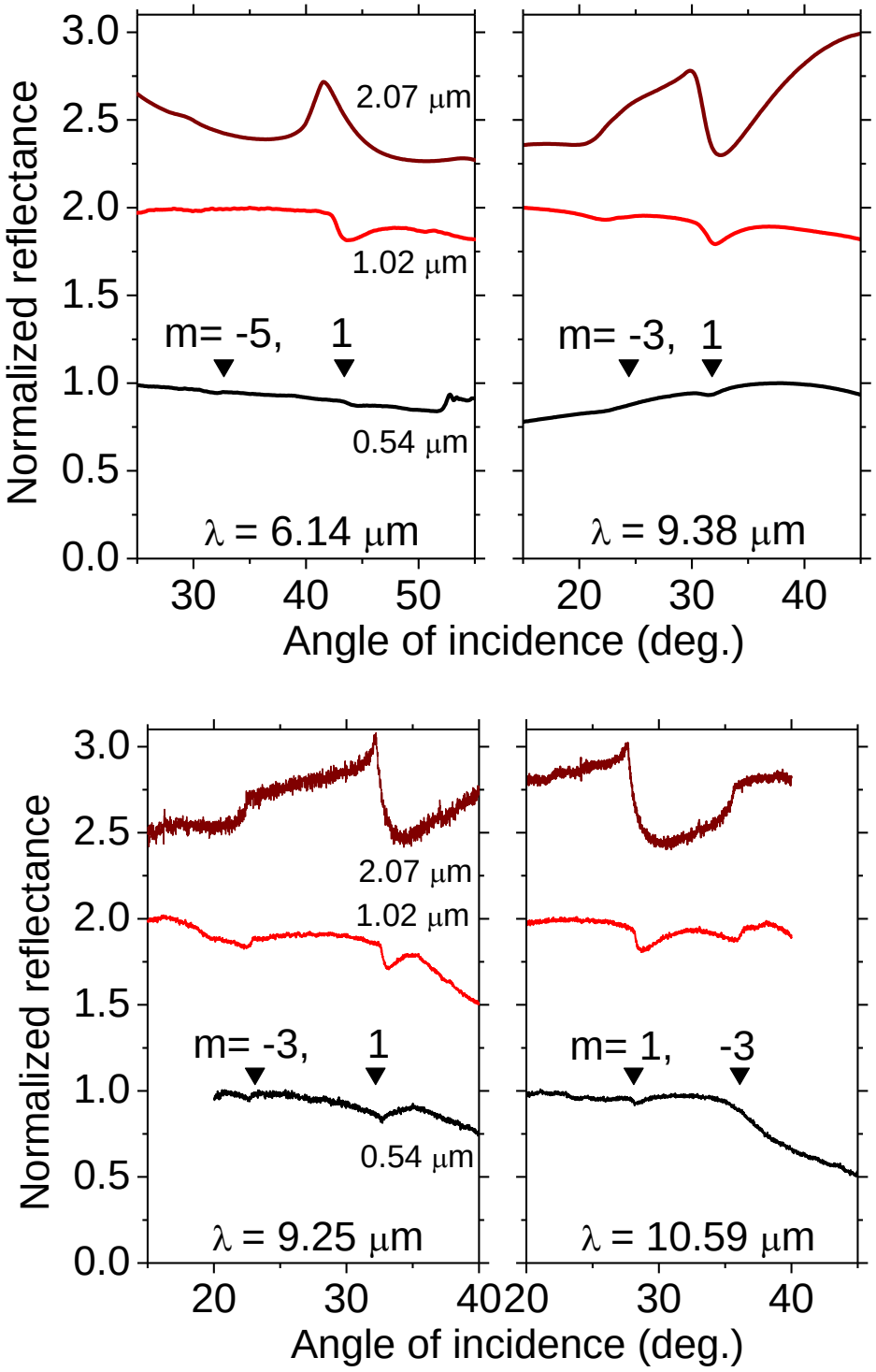

Figure 17: Angular reflectance spectra of Bi gratings at QCL (top) and CO2 laser (bottom) wavelengths.

The calculated SP energy decay length L_x, is presented in Figure 18 (upper) as a function of free-space photon wavelength. Our criteria for adequate SP propagation length $L_x > 2\lambda_{IR}$ is very well satisfied for Bi at all wavelengths. i.e. the surface waves are not weakly damped along the interface.

The characteristic penetration of the SPP electric field into the dielectric (in this case air) and into the conducting film are presented in Figure 18 (lower) were determined as functions of free space wavelength for Bi. Our criterion to be a useful SP-based sensor is $L_d < \lambda_{IR}$ which does not hold very well for Bi. The SP penetration depth into Bi is of the order of 1 to 10 μm, i.e comparable to the IR penetration depth. The mid IR wavelength we investigated for exciting SPs, from 3.4 to 10.5 μm, the penetration depth into air in the range 5-300 μm which poorly satisfies our criteria. Inflections are observed in propagation and penetration mode depth near where ε' changes sign at 30 μm wavelength.

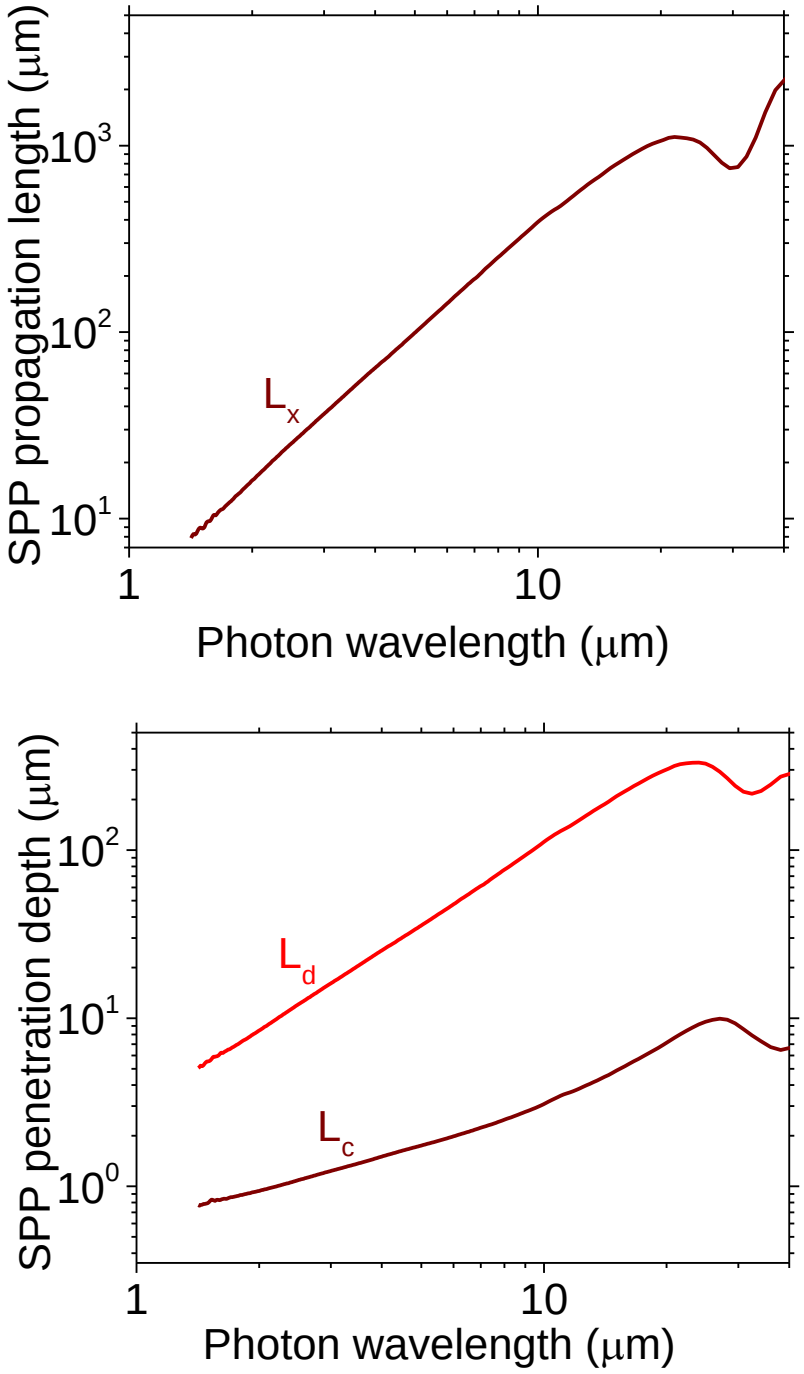

Figure 18: Energy propagation length as a function of free space wavelength (upper) and field penetration depths in air and conductor versus free space wavelength (lower) for surface polaritons on Bi.

4.4 Discussion

The usual condition for bound SPPs is that the real part of the permittivity be negative $\varepsilon' < 0$ and $|\varepsilon'| >> \varepsilon''$ [33]. In contrast, for Bi at the laser wavelengths used here, the ε' values are positive and $\varepsilon'' > |\varepsilon'|$. Nevertheless, clear resonances are observed in the angular reflectance spectra shown in Figure 17. These are attributable to SPs since similar measurements on the uncoated silicon gratings yield no resonances. Resonances do appear for Si gratings if the carrier concentration exceeds ~$3x10^{20}$ cm^{-3} [16]. Sensor applications mainly require the existence of any resonance that is sensitive to index changes above the grating. For such applications the question of whether the SP is bound or unbound is irrelevant. For applications such as plasmons wave guides, where long propagation and tight mode confinement are desired, Bi satisfies only the low loss propagation criterion in the LWIR.

In summary, plasmon resonances have been observed in the experimental reflection spectrum from Bi grating couplers. The wavelengths 3.4 μm to 10.5 μm were in the range of nominally unbound radiative SPs, and bound surface waves can be spoken of only because of the relatively large magnitude of ε'', which may cause rapid damping of the wave away from the surface. The possible resonances on optically thick films at 3.4 micron wavelength are not very distinct nor they clearly identifiable with SP generation. Better resonances are observed at longer wavelengths for optically thin films. Traditional SPPs may exist below 2.9 μm and above 30 μm wavelengths range where real part of permittivity is negative, though the imaginary part is still comparatively large.

CHAPTER FIVE: INFRARED SURFACE POLARITONS ON POLYANILINE

5.1 Introduction

Conducting polymers such as polyaniline and polypyrrole have plasma frequencies in the infrared wavelength range and show metallic characteristics [57 - 59]. In particular, they feature a permittivity whose real part is negative at sufficiently long wavelength, a condition for supporting a surface plasmon polaritons (SPPs) [59]. Polyaniline (PANI)-based conducting polymers have been investigated because of these unique electrical and optical characteristics which can be tuned by chemical doping.

In this paper, experimental and theoretical investigation of SPPs on a conducting polymer such as polyaniline doped with camphorsulphonic acid (PANI-CSA) was done. Polyaniline films were prepared, optical constants determined, and resonance spectra calculated using Hessel and Oliner theory [7]. The angular reflectance spectra of doped polyaniline were compared with already published experimentally measured permittivities. A specific goal is to identify conducting polymer having tight mode confinement, sharp reflectivity resonances, and capability to be functionalized for biosensor applications at infrared frequencies.

5.2 Experimental Details

Polyaniline was synthesized by making 1 mol /L aqueous HCl solution (pH between 0 and 2), ammonium persulfate as oxidant with an oxidant/ aniline (monomer) molar ratio ≤ 1.15 in order to obtain high conductivity and yield [60]. The monomer concentration was 0.1 mol/L. The solution temperature was 0°C in order to limit secondary reactions. The duration of the reaction was 2 h. Aqueous ammonium persulfate solution was added slowly drop by drop to the aniline/HCl solution. The mixture was stirred continuously during the whole reaction. The formed precipitate was removed by filtration and washed repeatedly with HCl and dried in an oven for 72 h. The obtained material was polyemeraldine salt, i.e. polyemeraldine hydrochloride (PANI-HCl), which has green color. It was secondary doped with 1 M aqueous solution of camphorsulfonic acid (CSA) [61] to increase conductivity. The obtained powder was washed and dried under vacuum for 48 h. Polyaniline (polyemeraldine) solutions of 10 and 16 wt % were prepared with solvent m-cresol. We spin-cast the polyaniline solution at 3000 and 2500 rpm for 0.5 and 1 min, respectively, to obtain different film thickness in different samples. Resistivity of the resulting film was measured using four contact method to be $\rho = 0.005\ \Omega$- cm.

To measure the infrared penetration depth, films of different thickness were deposited on un-doped double-side polished silicon. Transmission measurements were made using a Fourier spectrometer. Mechanical thickness was measured using atomic force microscopy near a scratch in the film. These measurements allowed us to determine the thickness needed in the subsequent ellipsometry measurements to avoid contributions from the substrate. Complex permittivities of

optically thick samples of polyaniline were determined using a J.A. Woollam IR-VASE in the wavelength range 1-40 micron.

The experimental permittivity values for polyaniline at laser wavelengths are given in Table 3, together with the relative surface impedance.

Table 3: Optical parameters of polyaniline.

	λ (μm)	ε′	ε″	ξ (Eq.3.4)
PANI	9.25	9.8848	20.04558	- *i* (0.1796 + i 0.1116)
	10.59	11.51792	20.64031	- *i* (0.1773 + i 0.1040)

5.3 Results

Figure 19 shows the raw ellipsometry spectra (ψ, Δ) at an incidence angle of 65 degree. Figure 20 presents permittivity spectra of polyaniline PANI-CSA calculated from the raw data (thick red curves above the zero line). Data from Reference [57] are plotted as symbols. Data for ε′ from Ref. [59] are plotted as a continuous curve that falls entirely below the zero line. Values of permittivity and surface impedance at our laser wavelengths are given in Table 3. The ε′ values for our PANI-CSA sample were positive for all infrared wavelengths investigated, indicating lower than desired conductivity. The values are reasonable considering that the resistivity of our film is 5x higher than for our p-Si whose ε′ is barely negative at 10 μm [16].

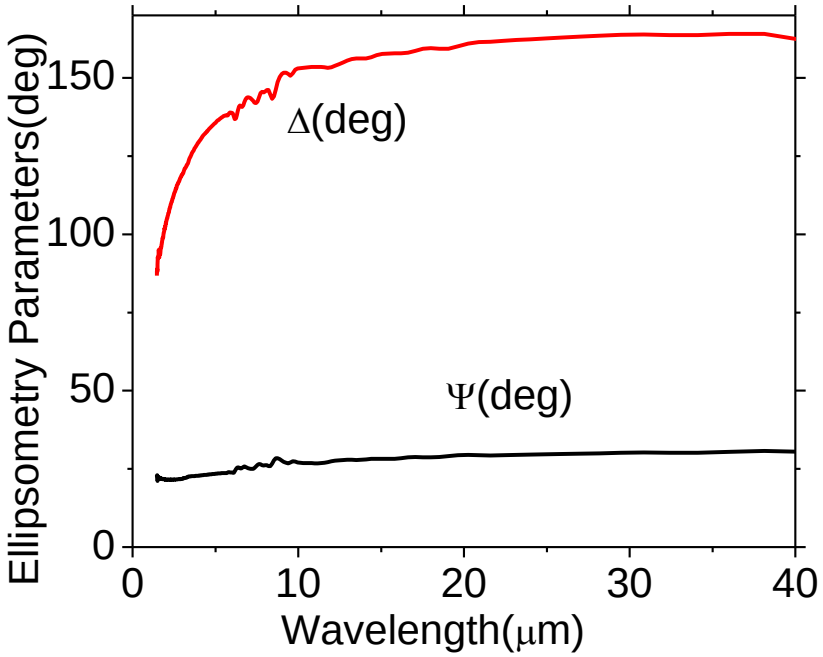

Figure 19: Raw ellipsometry data of PANI-CSA.

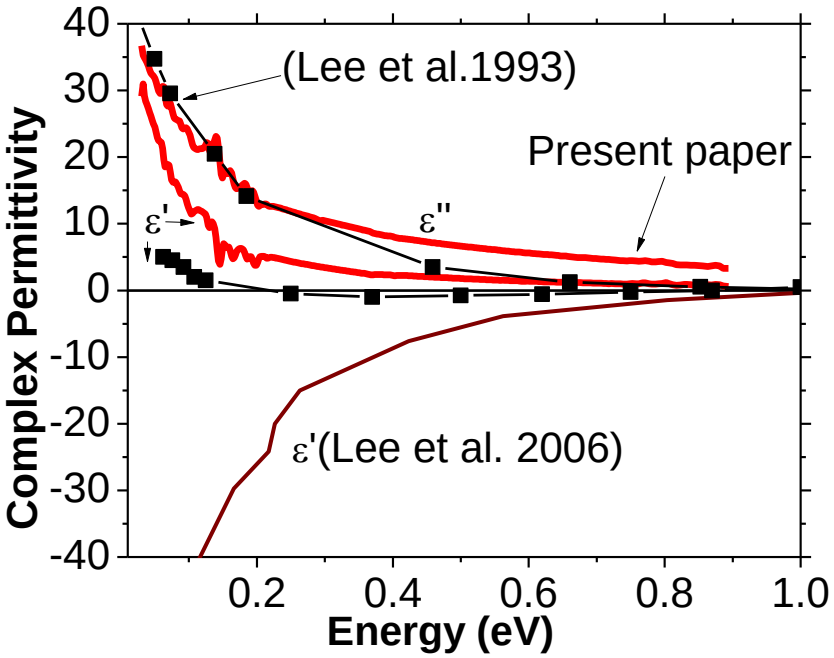

Figure 20: Real and imaginary part of permittivity for polyaniline from ellipsometry data, including published values from Refs. [57,59].

Ref. [57] values for ε′ are barely negative in the range 0.2 to 0.8 eV. Ref. [59] values go strongly negative for energies below 1 eV, which is characteristic of strongly metallic behavior. No ε″ spectrum is given in the Ref. [59] which is unique among published paper of having so strongly negative ε′ behavior more typical of a good metal. We regard those results with suspicion. Our data are more closely in agreement with the Ref. [57] results, though our permittivity never goes negative. We and Ref. [57] find $\varepsilon'' > \varepsilon'$, suggesting that useful SP excitation resonances are still possible, though they may be broad. The resistivity of our sample is 0.005 Ω-cm which is higher than the values $\rho = 0.000769$ and 0.0029 Ω-cm from Refs. [57] and [59], respectively. It is curious that the most strongly negative ε′ data is for a sample intermediate in resistivity value, and this again causes us to question the validity of the Ref. [59] results. The resistivity of the sample is 1000x greater than the good metals, while the permittivity is similar to that of a good metal, a highly suspicious thing. As a minimum comparison of the different reports emphasizes how variable conducting polymers can be in their optical properties.

The IR-field penetration depth into the conductor, δ, was determined from the permittivity using Eq. (2.10) to be ~ 4 microns at ~ 10 micron wavelengths. This value was qualitatively confirmed by FTIR spectrum of a spin-cast polyaniline film of 5 μm thickness on double side polished silicon. This transmission spectrum is presented in Figure 21. The transmittance is almost zero across the middle infrared, in agreement with expectations from the estimated IR penetration depth.

If optically thick films are required for applications, then preparation of high quality films may be challenging, as was found in our experience. Such thick films tend to crack as the solvent dries and they stick poorly to substrate especially Si.

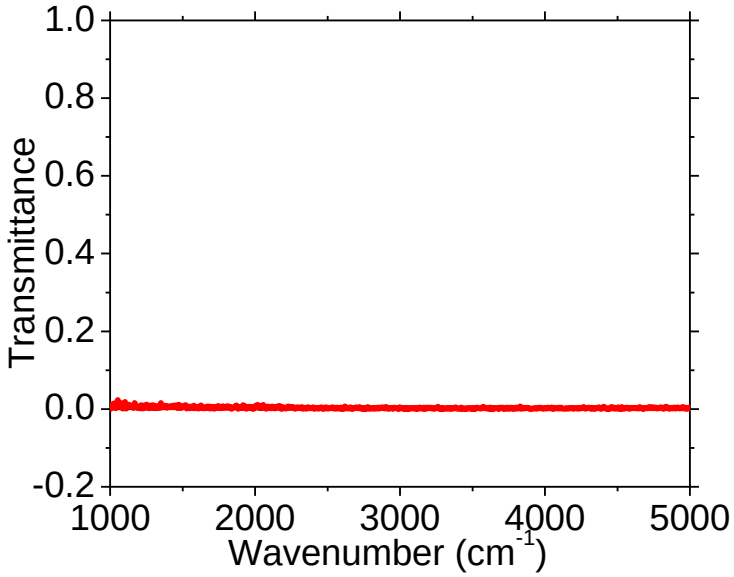

Figure 21: FTIR Spectrum of 5 μm thick Polyaniline Film.

Expected resonance angles and the angular reflectance spectra are calculated using the ε′ and ε″ values using M = 1 in Hessel and Oliner resonance formula Eq. (3.7) [16]. Figure 22 presents the calculated reflectance spectra of SPPs for our measured and the most optimistic published [59] permittivity values at λ = 10.59 μm. In our case the ε′ value is slightly positive, yet SP surface waves exist and their excitation resonance is observed anyway because ε″ > ε′. The resonance based on Ref. [59] data is sharper than the one based on our data, although that calculation is based on zero loss for absence of an ε″ value. The resonance angle for our

measured permittivity is 29.65 deg. which differs by 0.35 deg. from the resonance angle determined using the published permittivity.

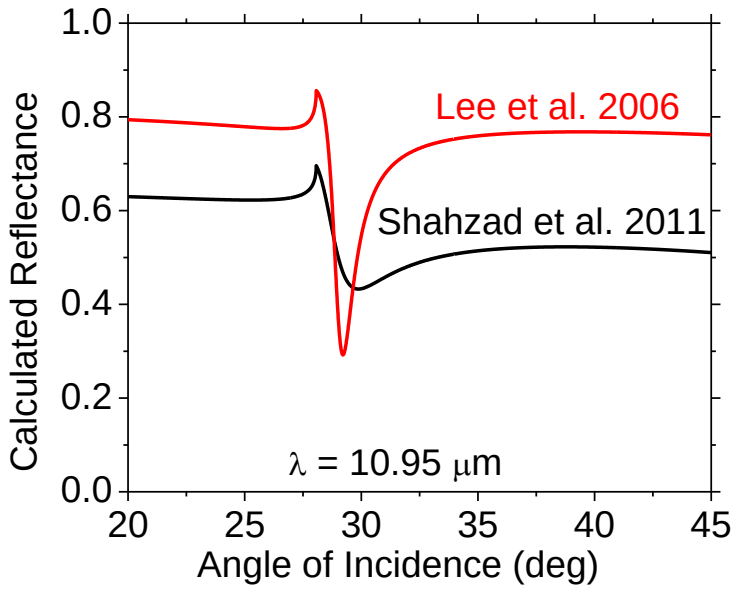

Figure 22: Comparison between calculated angular reflectance spectra of using our measured and the published [59] IR-ellipsometry data of polyaniline film.

The characteristic penetration of the SPP electric field into the dielectric (in this case air) and into PANI-CSA film are presented in Figure 23 were determined as functions of free space wavelength. PANI supports bound surface wave over the entire range 1-40 μm because $\varepsilon'' > \varepsilon'$ everywhere [19]. For $\lambda > 10$ μm, the extent of the E-field above the surface starts to exceed the free space wavelength. For $\lambda < 10$ μm, the extent is slightly less.

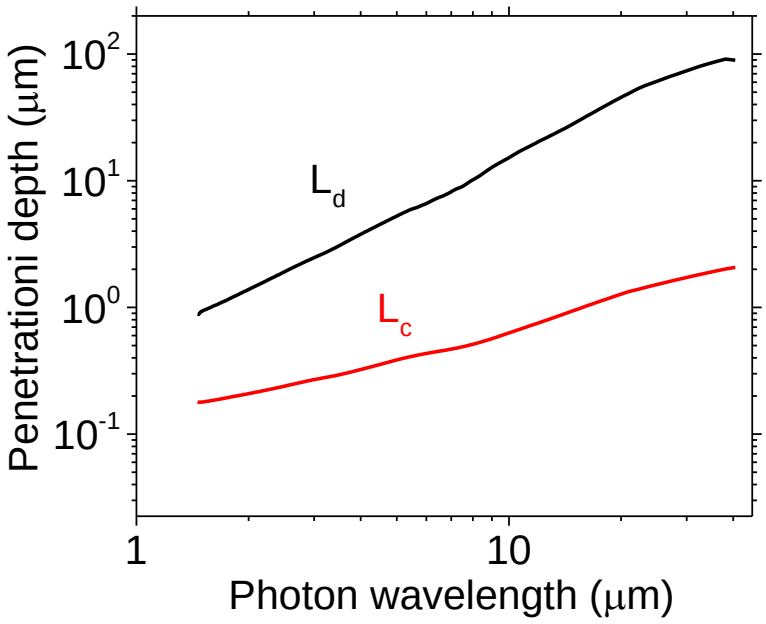

Figure 23: Field penetration depths in air and conductor versus free space wavelength for surface polariton on PANI-CSA film

5.4 Summary

Calculated SPP resonances on the conducting polymer polyaniline were presented. Results show resonances that should be sensitive to changes in the refractive index above their surfaces and hence should have potential to be used as the SPP hosts with sufficient mode confinement for IR sensor applications. Unfortunately, we were unable to achieve fabrication of smooth large area optically thick films on grating substrates for direct experimental investigations of SPs.

CHAPTER SIX: SURFACE POLARITONS ON POLYANILINE-GRAPHITE COMPOSITES

6.1 Introduction

We studied optical properties and SPP resonances for of composites of polyaniline (PANI) and graphite. The conductivity of the composite can exceed that of either the graphite or polyaniline alone [62] and hence may have mid-IR plasma frequency.

6.2 Experimental Details

Polyaniline-graphite composite was synthesized by making 1 mol/L aqueous HCl solution (pH between 0 and 2). Ammonium persulfate was used as oxidant with an oxidant/aniline (monomer) molar ratio ≤ 1.15. The colloidal and nano-graphite with average particle size less than 0.5 microns were added according to the amount desired in the final product [61-63]. The aniline (monomer) concentration was 0.1 mol/L. The solution temperature was 0°C in order to limit secondary reactions. The duration of reaction was 2 h. Aqueous ammonium persulfate solution was added slowly drop by drop to the aniline-graphite/HCl solution. The mixture was stirred continuously during the whole reaction. The formed precipitate was removed by filtration and washed repeatedly with HCl solution and dried for 48 h. It was secondarily doped with 1 M aqueous solution of HMSA (methanesulfonic acid). The obtained product was washed and dried under vacuum for 48 h. Resistivity of pressed pellet of the composite material was measured using four contact method to be as low as $\rho = 0.005\ \Omega$-cm.

The highest conductivity measured was 200 S/cm for 90/10 mass ratio of PANI-graphite composite. The conductivity of the composite is higher than the individual constituents of the composite, 154 S/cm and 10 S/cm for pristine graphite powder and polyaniline, respectively. By changing the mass ratio of the two components, an increase in electrical conductivity was detected. This is due to intercalation of polyaniline chain inside graphite particles, which facilitates charge transfer [63].

For spin-casting of films, polyaniline-graphite solutions of 5 and 10 wt % were prepared with solvent m-cresol and N-Methyl-2-pyrrolidinone (NMP). We spin-cast the polyaniline-graphite solution at 3000 and 2500 rpm for 0.5 and 1 min, respectively, to obtain different film thicknesses in different samples. DC conductivities were measured using four contact methods. The conductivities of the composite thin film in organic solvent turned out to be less than the conductivities in powdered form.

To measure the infrared penetration depth, films of different thicknesses were deposited on un-doped double-side polished silicon. Transmission measurements were made using a Fourier spectrometer. Mechanical thickness was measured using atomic force microscopy near a scratch in the film. These measurements allowed us to determine the thickness needed in the subsequent ellipsometry measurements to avoid contributions from the substrate. Complex permittivity of PANI-graphite optically thick film in m-cresol and NMP were determined in wavelength range 1-40 micron.

6.3 Results

Table 4: Optical parameters of polyaniline-graphite composites. Permitivitties and complex surface impedances are given at 9.25 micron wavelength.

Composite materials	ρ (Ω-cm)	ε′	ε″	ξ [Eq.(3.4)]
PANI/CGP in m-cresol	0.056	3.1343	4.1371	0.3948 – i0.1954
PANI/CGP in NMP	0.166	1.8712	3.1570	0.4535 - i0.2584
PANI/NGP in m-cresol	0.337	3.5557	3.2682	0.4240 - i0.1652

Figure 24 present micro-Raman spectra of the polyaniline emeraldine salt (ES). The major peaks are labeled with their frequencies. The Raman spectra of ES polyaniline show the vibrational modes at 800, 1180, and 1300-1600 cm^{-1}. For composite materials of polyaniline-colloidal graphite (PANI/CGP) and polyaniline nano-graphite (PANI/NGP), the vibrational modes of PANI were detected at the same positions and were not affected by the presence of graphite. Two vibrational modes around 1500 and 2700 cm^{-1} coincide with the first and second order Raman spectrum of graphite. These peaks match the published data [62] as shown in Figure 24 (bottom) for the micro Raman spectra of polyaniline, pristine graphite powder and the composite of PANI-Graphite.

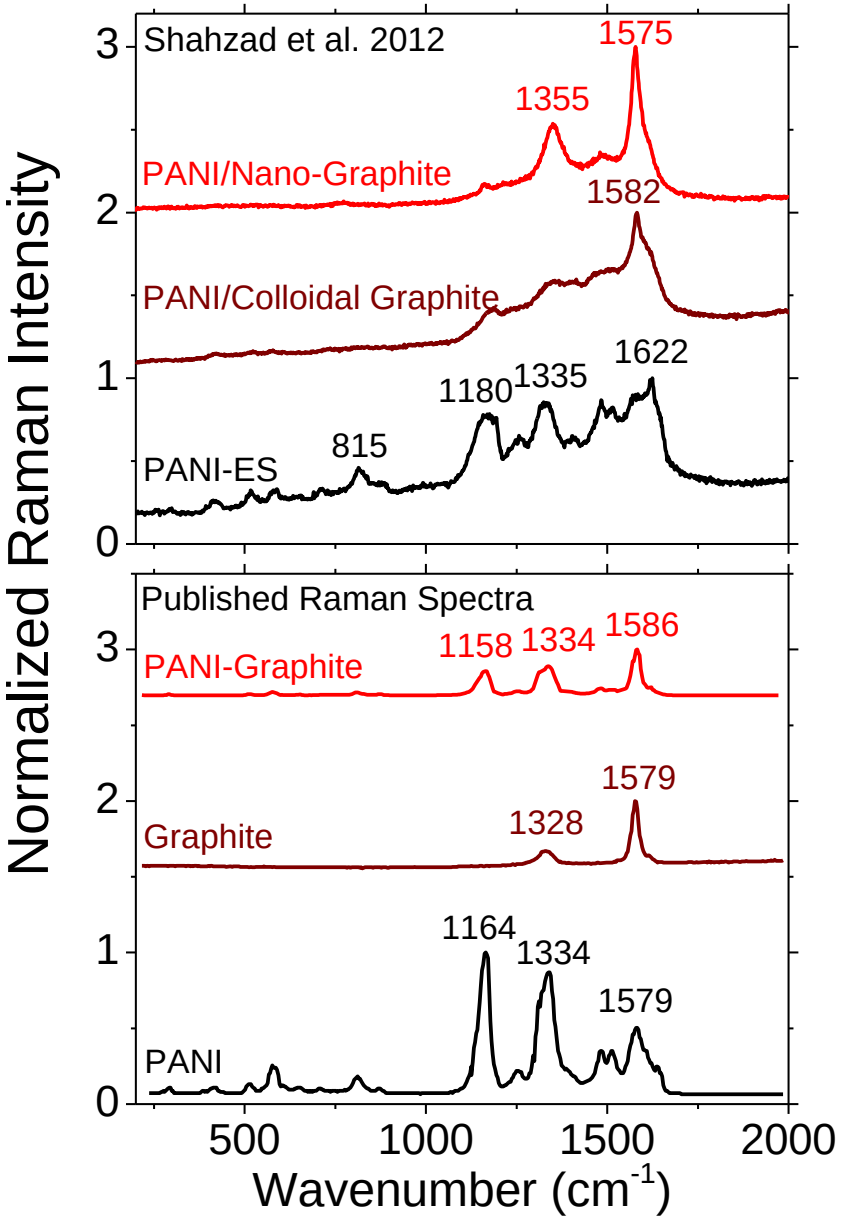

Figure 24: Measured micro-Raman spectra (top) of polyaniline emeraldine salt (PANI-ES), polyaniline-graphite composites and published data (bottom).

Published data of both PANI and Graphite Raman spectra have a peak at 1579, but in the composite material, this peak is shifted or replaced by one at 1586 cm^{-1}. This peak is higher than the 1575 and 1582 cm^{-1} peaks in composite prepared as shown in Figure 24 (top). It is difficult to understand how a peak common to both materials is shifted in the composite, unless there is a dependence of the Raman spectrum on the Fermi level [64].

Figure 25 presents the raw ellipsometry spectra (ψ, Δ) in the wavelength range 1-40 micron at incidence angle of 75° for each composite prepared. These data are used to calculate the permittivity using Eqs. (2.16) and (2.17). Figure 26 presents a plot of the real part of complex permittivity for the colloidal-graphite (CGP) and nano-graphite (NGP) composites with polyaniline in NMP and m-cresol. Contrary to expectations that motivated our investigations of composites, the real part of the permittivity never goes negative in this wavenumber range.

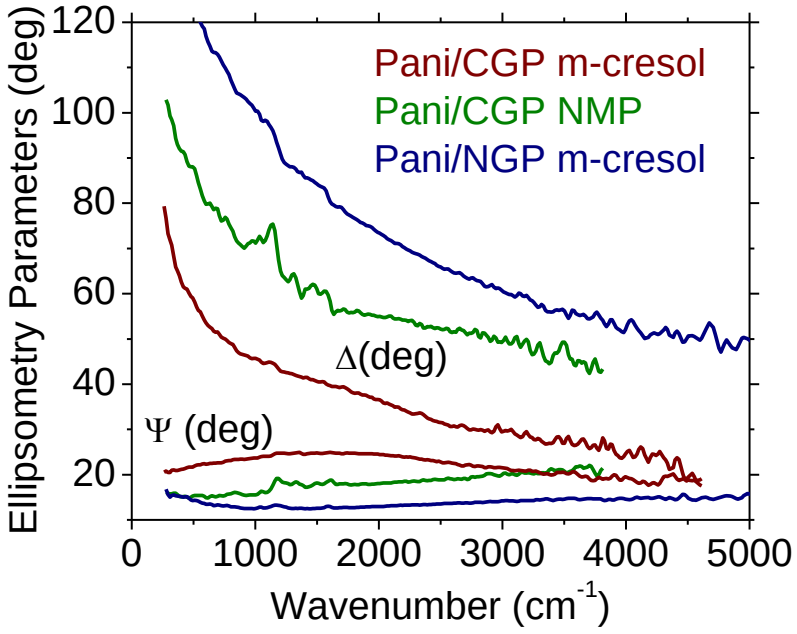

Figure 25: Raw ellipsometry data for polyaniline graphite composites in various organic solvents.

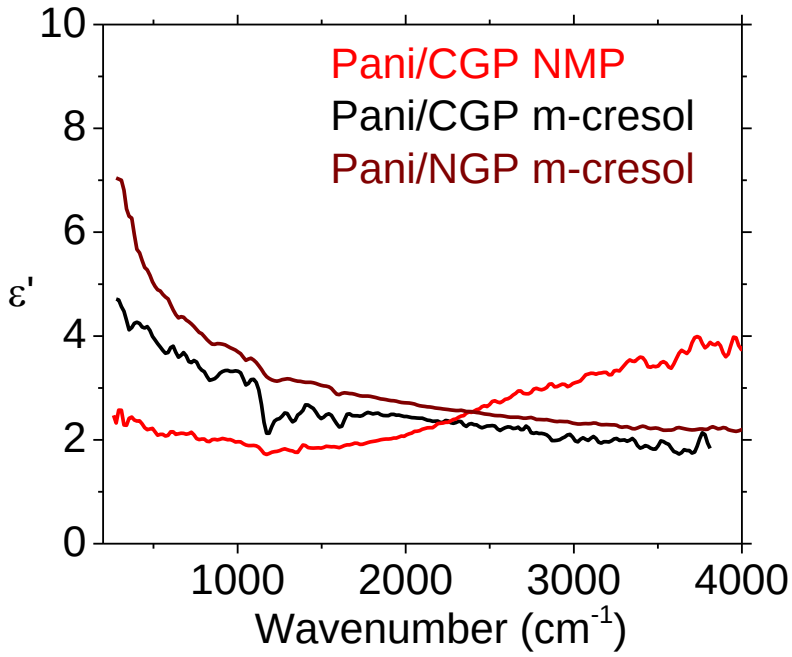

Figure 26: Real part of IR permittivity of polyaniline graphite composite in various organic solvents.

Figure 27 presents the imaginary part of complex permittivity of same composite materials in various organic solvents for conducting polymers. The imaginary part of the permittivity always exceeds the real part. These conditions in principle still permit the appearance of a bound surface wave that is qualitatively similar to an SPP [19].

In all cases the ε′ values are positive, though bound surface waves can still occur when ε″ > ε′. We note that for all samples the imaginary part of the permittivity follows the expected behavior, i.e. it is positive and it trends like 1/frequency, as expected for conductors. The behavior of the real part is more difficult to explain, since for a conductor it should become negative at some point in going toward low frequencies and then continue heading toward larger negative values. None of the plots having ε′ show such behavior.

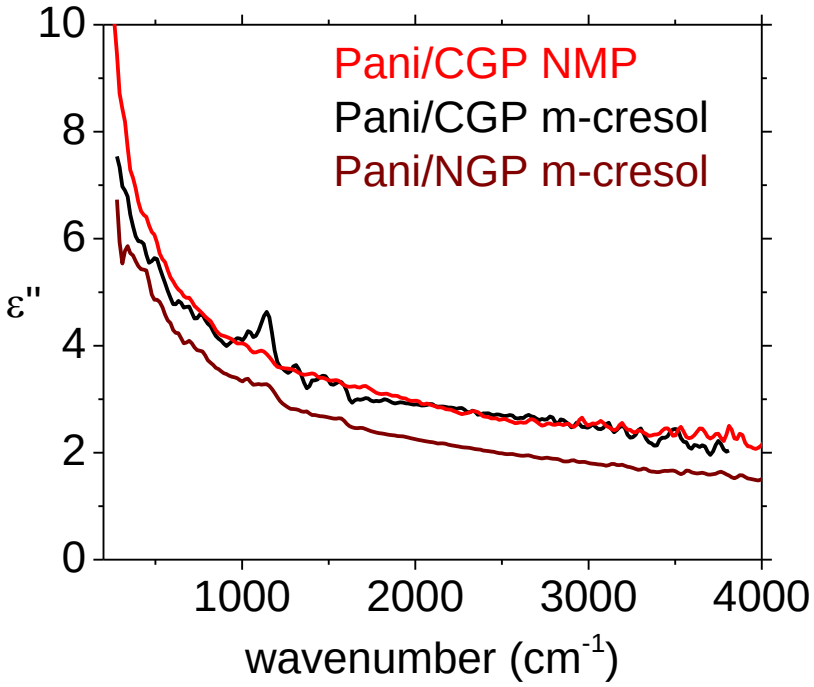

Figure 27: Imaginary part of the infrared complex permittivity of polyaniline graphite composites in various organic solvents.

The IR-field penetration depth δ into composite material was determined using Eq. (2.15) to be 5 microns at 9.25 micron wavelength. This value was qualitatively confirmed by FTIR spectrum of a spin-cast film of composite material on double polished silicon. The spectrum in the range 2-10 micron wavelength is presented in Figure 28. The transmittance is very low, almost zero for 5-micron-thick film across the mid infrared which is in agreement with expected IR penetration depth.

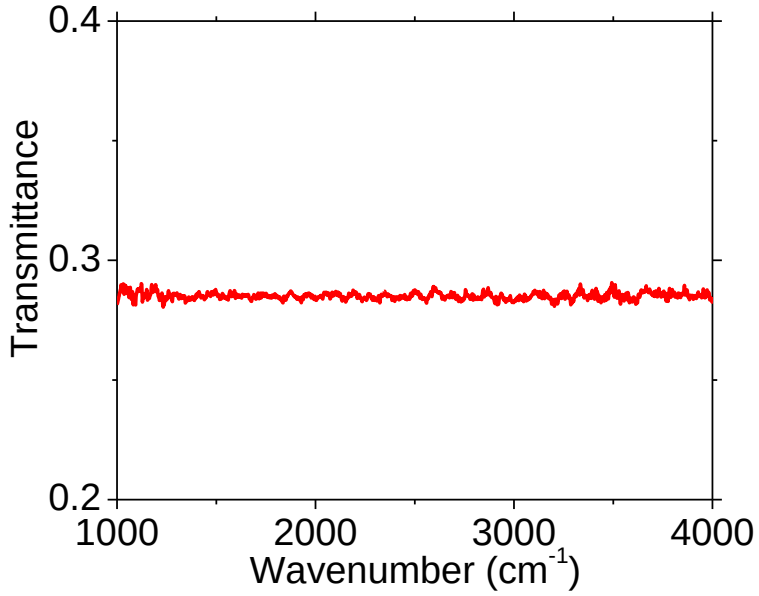

Figure 28: FTIR spectrum of 5 μm thick polyaniline-graphite composite.

Expected resonance angles and the angular spectra are calculated using the ε′ and ε″ values according to Eqs. (3.1) and (3.7), assuming a 20 micron period grating and using M = 1. Figure 29 presents the calculated reflectance spectra of SPPs for composite material thin film in two different organic solvent. For good conductors, we expect to see a sharp deep resonant decrease at a particular angle, usually asymmetric and with a cusp on one side. When the amplitude of the grating is too high, the imaginary part of the permittivity is too large, or the real part is too small or positive, the resonance is broadened, and only the cusp remains sharp. We see such a cusp in the calculated reflectance spectrum of composite material prepared at around 32 deg. However, there is no clear resonance. Moreover, the quality of the spin-coated films, when they were thick enough to be optically thick, was too poor to allow specular reflectance measurements.

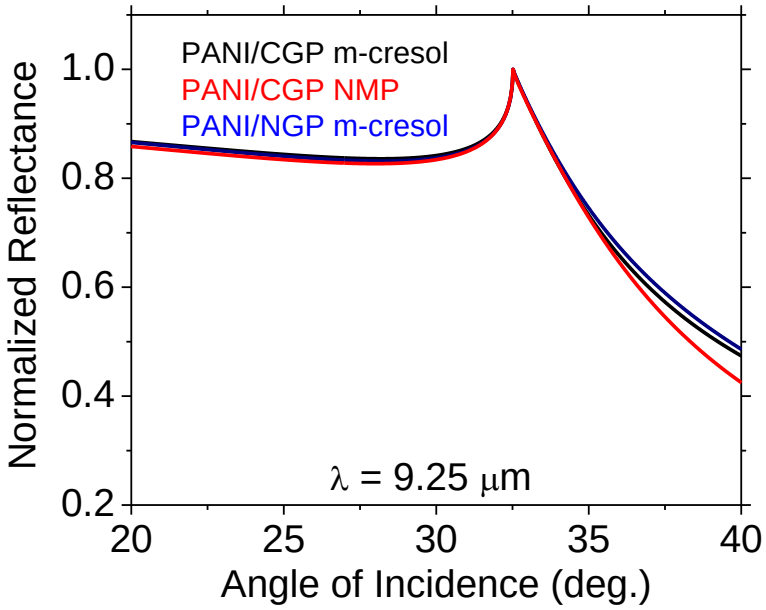

Figure 29: Calculated angular reflectance spectra for 20 micron period gratings and p-polarized 9.25 μm wavelength incident IR beam.

6.4 SUMMARY

IR permittivity data was presented for spin-coated composites of conducting polymer and graphite. Results show small positive values across the spectrum for both real and the (generally larger) imaginary parts. Under such conditions bound surface waves are possible, in principle. However, calculated resonance spectra fail to indicate the presence of useful surface-wave excitation resonances for gratings formed from these materials. Due to poor film quality for optically thick films, experimental investigations of surface plasmon resonance were impossible.

CHAPTER SEVEN: CONCLUSIONS

This dissertation focused on extension of surface plasmon applications into the IR by exploiting the optical properties of materials with carrier concentrations ~2 orders smaller than usual noble metals. The materials studied were heavily-doped silicon, the semi-metal bismuth, and semiconducting polymers. IR surface plasmon excitation resonances were investigated using gratings made of three materials.

Doped Silicon with carrier concentrations of 10^{20} cm^{-3} is best suited for SPP applications in the long-wave IR (6-12 microns) with adequate mode confinement while maintaining an acceptable propagation length.

Long-wave IR surface wave excitations were observed on Bi gratings near 10 microns wavelength where our measured ε' is positive but small, while $\varepsilon'' > \varepsilon'$. However the resonances are broad and the quality of the surface of evaporated Bi film is poor, so this material appears less promising than Si. Moreover, Bi film needs to be at least 6 μm thick to be optically thick. The infrared permittivity that we measured for evaporated Bi film differs significantly from previously published results for melt-cast or single crystal bulk Bi. The differences are worth further investigations. Since light doped silicon does not show SPR so Bi may be used as a host for SPR based sensor.

Conducting polymers (Polyaniline-CSA) and its composites (Polyaniline-Graphite) were prepared and their optical properties determined. We did not succeed in achieving negative ε' in the infrared for any of them. For polyaniline, ε' was sufficiently smaller than ε'' and

calculations do show a surface wave excitation resonance that may have practical value. However, for the composite, the two parts of the permittivity were comparable, and calculations did not yield a useful resonance. Our measured data of complex permittivity values cast suspicion on the report in Refs. [57, 59] of a near IR plasma frequency for polyaniline, an observation never repeated before or since by other research groups, to our knowledge. This is worth further investigations.

In conclusion, of the materials studied in my dissertation, heavily doped silicon appears to have the best promise for IR sensor applications based on surface plasmon resonances.

APPENDIX A: SEM IMAGES OF BISMUTH FILMS ON SILICON GRATINGS

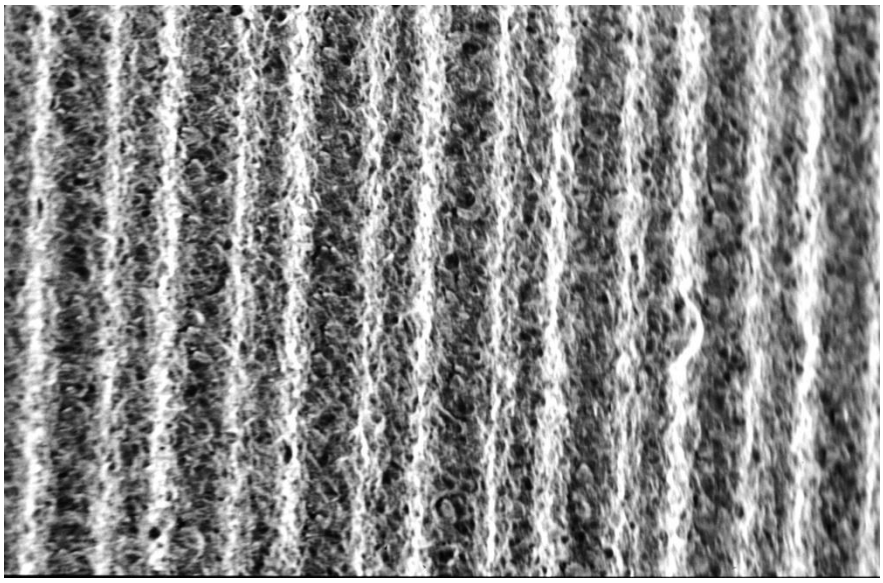

Figure 30: SEM image of optically thick Bi film on silicon gratings substrate with 50% duty cycle, 20 μm period and 4 μm amplitude.

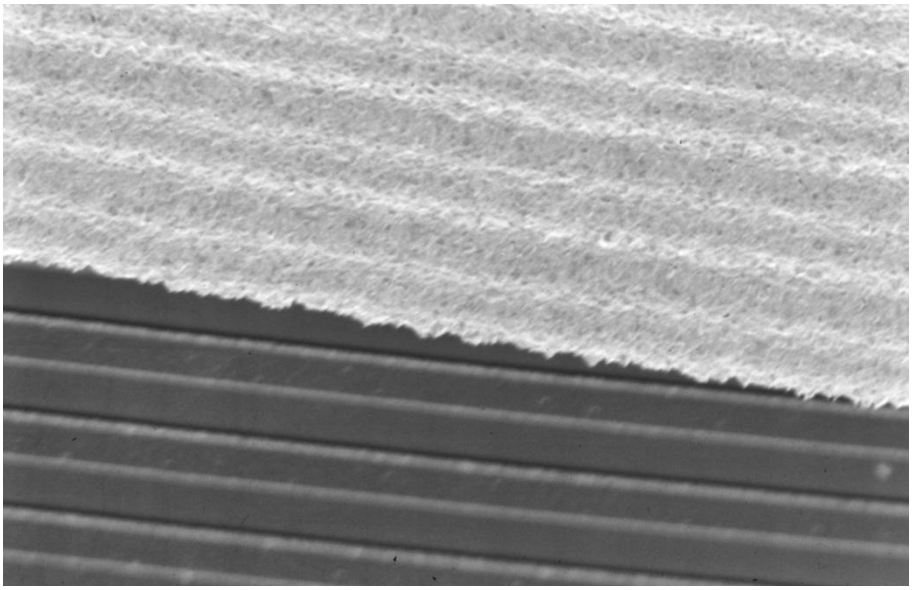

Figure 31: Bi-coating on the underlying grating structure with coating partially removed.

APPENDIX B: PUBLICATIONS

Journal:

1. Monas Shahzad, Gautam Medhi, Robert E. Peale, Walter R. Buchwald, Justin W. Cleary, Richard Soref, Glenn D. Boreman and Oliver Edwards, 'Infrared surface plasmons on heavily doped silicon', Journal of Applied Physics, **110**, 123105-6, (2011).
2. Justin W. Cleary, Gautam Medhi, Monas Shahzad, Imen Rezadad, Doug Maukonen, Robert E. Peale, Glenn D. Boreman, Sandy Wentzell, and Walter R. Buchwald, 'Infrared surface polaritons on antimony', Optics Express **20**, 2693-2705, (2012).
3. Monas Shahzad, Farnood K. Rezaie, Gautam Medhi, Chris J. Friedricson, Justin W. Cleary, Imen Rezadad, Robert E. Peale, Glenn D. Boreman, and Walter R. Buchwald, 'Infrared surface polaritons on bismuth', (in preparation).

Conference Proceedings:

1. Monas Shahzad, Gautam Medhi, Robert E. Peale, Ryuichi Tsuchikawa, Masahiro Ishigami, Walter Buchwald, Justin Cleary, Glenn D. Boreman, Oliver Edwards, D. J. Diaz, and Ted. A. Gorman, "Infrared surface waves on semiconductor and conducting polymer", Proc. SPIE 8024- 2 V. 7 (2011).
2. Monas Shahzad, Gautam Medhi, Doug Maukonen, Mehmet Yesiltas, Robert E. Peale, Walter R. Buchwald, Justin Cleary, Yi Liao, Candace Alber, Valentine K. Johns, Rahul Hegishte, Glen D. Boreman, "Infrared surface plasmon polariton on polyaniline-graphite composite ", Proc. SPIE 8366 – 3 V.6 (2012).

3. Christopher J. Fredricksen, Justin W. Cleary, Walter R. Buchwald, Pedro Figueiredo, Farnood Khalilzadeh-Rezaie, Gautam Medhi, Imen Rezadad, Monas Shahzad, Mehmet Yesiltas, Janardan Nath, Javaneh Boroumand, and Robert E. Peale, 'Planar integrated plasmonic mid-IR spectrometer', Proc. SPIE 8353 - 63 (2012).

REFERENCES

[1] R. W. Wood, "On a remarkable case of uneven distribution of light in a diffraction grating spectrum," Phil. Mag. **4**, 396-402, (1902).

[2] Lord Rayleigh, "On the dynamical theory of gratings," Proc. Roy. Soc. London A **79**, 399-416, (1907).

[3] U. Fano, "The theory of Anomalous Diffraction gratings and quasi-stationary waves on metallic surface (Sommerfeld's waves)," JOSA, **31**, 213-222, (1941).

[4] Pine and Bohm, "A collective description of electron interaction: III Coulomb Interactions in a Degenerate Electron Gas," Phy. Rev. **92**, 609-625, (1953).

[5] R. H. Ritchie, "Plasma losses by fast electrons in thin films," Phys Rev. **106,** 874-881, (1957).

[6] Richard A Ferrel, "Predicted radiation of plasma oscillations in metal film," Phys. Rev. **111**, 1214-1222, (1958).

[7] A. Hessel and A. A. Oliner, "A new theory of Wood's anomalies on optical gratings," Appl. Opt. **4**, 1275-1297, (1965).

[8] R. H. Ritchie, E. T. Arakawa, J. J. Cowan, and R. N. Hamm, "Surface plasmon resonance effect in grating diffraction," Phys. Rev. Lett. **21**, 1530-1532, (1968).

[9] A. Otto, "Excitation of non-radiative surface plasma waves in silver by method of frustrated total reflection," Z. Phys **216**, 319-410, (1968).

[10] E. Kretschmann and H. Raethers, "Radiative decay of non-radiative surface plasmon excited by light," Z. Naturrf, **234**, 2135-2136, (1968).

[11] M. L. Brongersma and P. G. Kik, *Surface Plasmon Nanophotonic*s (Springer, Berlin 2007).

[12] D. Sarid, and W. Challener, *Modern Introduction to Surface Plasmons, Theory, Mathematica Modeling, and Applications*, Cambridge Univ. Press (2010).

[13] W. Andrew Murray and William L. Barnes, "Plasmonics Materials," Adv. Mater, **19**, 3771-3782, (2007).

[14] J. A. Dionne and Harry A. Atwater, "Plasmonics: Metal-worthy methods and materials in nanophotonics," MRS Bulletin **37**, 717-724, (2012).

[15] J. C. Ginn, R. L. Jarecki, Jr., E. A. Shaner, and P. S. Davids, "Infrared plasmons on heavily-doped silicon," J. Appl. Phys. **110**, 043110-6, (2011).

[16] M. Shahzad, G. Medhi, R. E. Peale, W. R. Buchwald, J. W. Cleary, "Infrared surface plasmons on heavily doped silicon," J. Appl. Phys. **110**, 123105-6, (2011).

[17] D. Li, C. Z. Ning, "All semi-conductor active plasmonics system in mid-infrared wavelength," Optics Express, **19**, 14594-14603, (2011).

[18] S. Law, D. C Adams, A. M. Taylor, and D. Wasserman, "Mid-infrared designer metals," Optics Express, **20**, 12155-12165, (2012).

[19] J. W Cleary, G. Medhi, M. Shahzad, R. E. Peale, "Infrared surface polaritons on antimony," Optics Express, **20**, 2693-2705, (2012).

[20] R. Kiebooms, R. Menon, K. Lee, *Handbook of Advanced Electronic and Photonic Materials and Devices,* 8, Ch. 1, "Synthesis, electrical, and optical properties of conjugated polymers," 1-102, (2001).

[21] P. R. West, S. Ishii, G. V. Naik, N. K. Emani, V. M. Shalaev, and Alexandra Boltasseva, "Searching for better plasmonic materials," Laser Photonics Rev. **4**, 795-808, (2010).

[22] R. Stanley, "Plasmonics in the mid-infrared," Nature Photonics **6**, 409-411, (2012).

[23] www.plaisir-project.eu.

[24] A. Boltasseva, and H. A Atwater, "Low-Loss plasmonic metamaterials," Science **331** 290-291, (2011).

[25] Alan J Heeger, Niyazi S. Sariciftci, Ebinazar B. Namdas, *Semiconducting and Metallic polymers* (Oxford Univ. Press, 2010).

[26] H. Raether, *Surface Plasmons on Smooth and Rough Surfaces and on Gratings* (Springer-Verlag, Berlin, 1988).

[27] H. A. Atwater, "The Promise of Plasmonics," Scientific American Magazine, March 18th, (2007).

[28] R. E. Peale, J.W. Cleary, W. R. Buchwald, O. Edwards, "Infrared surface plasmon resonance biosensors," Proc. SPIE 7673-5, (2010).

[29] H. G. Tompkins, *A user's guide to ellipsometry* (Academic, San Diego, 1993).

[30] P. Y. Yu and M. Cardona, *Fundamental of Semiconductors* (Springer, Berlin, 1996).

[31] J. B Khurgin and A. Boltasseva, "Reflection upon the losses in plasmonics and metamaterials," MRS Bulletin **37**, 768-779, (2012).

[32].L. D. Landau, E. M. Lifshitz, and L. P. Pitaevskii, *Electrodynamics of Continuous Media*, 2nd ed, (Elsevier Butterworth Heinemann, Amsterdam, 1993).

[33] S.A. Maier, *Plasmonics: Fundamentals and Applications* (Springer, New York, NY, 2007).

[34] J. Homola, S. S Yee, and G. Gauglitz, "Surface plasmon resonance sensors: review," Sensor and Actuators B: Chemical Vol.**54**, 3 3-15 (1999).

[35] S. Patskovsky, A. V. Kabashin, M. Meunier, and J. H. T. Luong, "Properties and sensing characteristics of surface-plasmon resonance in infrared light," J. Opt. Soc. Am. A **20**, 1644-1650, (2003).

[36] J. N. Yih, Y. M. Chu, Y. C. Mao, W. H. Wang, F. C. Chien, C. Y. Lin, K L. Lee, P. K. Wei, and S. J. Chen, "Optical waveguide biosensors constructed with subwavelength gratings," Appl. Opt. **45,** 1938-1942, (2006).

[37] R. Ziblat, V. Lirtsman, D. Davidov, and B. Aroeti, "Infrared surface plasmon resonance: a novel tool for real time sensing of variations in living cells," Biophys. J. **90**, 2592-2599, (2006).

[38] J. W. Cleary, R. E. Peale, D. Shelton, G. D. Boreman, R. Soref, W. Buchwald, "Silicides for infrared surface plasmon resonance biosensors," Proc. Mat. Res. Soc. 1133-AA 10-03, (2008).

[39] R. Soref, R. E. Peale, and W. Buchwald, "Longwave plasmonics on doped silicon and silicides," Opt. Express **16**, 6507-6514, (2008).

[40] J. W. Cleary, R. E. Peale, D. J. Shelton, G. D. Borman, C. W. Smith, M. Ishigami, R. Soref, A. Drehman and W. R. Buchwald, "IR permittivities for silicides and doped silicon," J. Opt. Soc. Am. B **27**, 730-734, (2010).

[41] S. Basu, B. Lee, and Z. Zhang, "Infrared radiative properties of heavily doped silicon at room temperature," J. Heat Transfer **132**, 023301-8, (2010).

[42] Y. -B. Chen, "Development of mid-infrared surface plasmon resonance-based sensors with highly-doped silicon for biomedical and chemical applications," Optics. Express **17**, 3130-3140, (2009).

[43] W. DiPippo, Bong Jae Lee, and Keunhan Park, "Design analysis of doped-silicon surface plasmon resonance immunosensors in mid-infrared range," Optics. Express **18**, 19396-19406, (2010).

[44] M. Shahzad, G. Medhi, R. E. Peale, R. Tsuchikawa, M. Ishigami, W. Buchwald, J. W. Cleary, G. D. Boreman, O. Edwards, D. J. Diaz, and T. A. Gorman, "Infrared Surface plasmon on doped silicon and conducting polymers," Proc. SPIE **8024,** 80240B, (2011).

[45] J. W. Cleary, G. Medhi, R. E. Peale, and W. Buchwald, "Long wave infrared surface plasmon grating coupler," Vol. **49,** 3102-3110, (2010).

[46] E. B. Saff and A. D. Snider, *Fundamentals of complex analysis with applications to engineering and science*, 3rd Ed. (Pearson Education, Upper Saddle River, New Jersey, 2003).

[47] S. M. Sze, *Physics of Semiconductor Devices*, 2nd Ed. (Wiley-Interscience, New York, 1981).

[48] A. R. Brown, G. Roy and A. Asenov, "Poly-Si-Gate-related variability in decananometer MOSFETs with conventional architecture," IEEE Trans. Electron Devices **54**, 3056 (2007).

[49] M. V. Fischetti and S. E Laux, "Band structure, deformation potentials, and carrier mobility in strained Si, Ge, and SiGe alloys," J. Appl. Phys. **80,** 2234 -2252, (1996).

[50] A. Brillante, I. Pockrand, M. R. Philpott and J. D. Swalen, "Experimental observation of exciton surface polaritons on a polymerized diacetylene crystal," Chem. Phys. Lett. **57**, 395-399, (1978).

[51] F. Yang, G. W. Bradberry and J. R. Sambles, "Experimental observation of surface exciton-polaritons on Vanadium using infrared radiation," J. Mod. Optic. **37**, 1545-1553, (1990).

[52] F. Yang, J. R. Sambles, and G. W Bradberry, "Long range surface modes supported by thin films," Phys. Rev. B **44**, 5855-5872, (1991).

[53] A. Shivola, J. Qi, I. V. Lindell, "Bridging the gap between plasmonics and Zenneck waves," IEEE Antennas and Propagation Mag. Vol. **52**, 124-136, (2010).

[54] Y Fuzi, G. W. Bradberry and J. R Sambles, "Infrared surface plasmons-polaritons on Ni, Pd, Pt," J. Mod. Opt. **36**, 1405-1410, (1989).

[55] J. N Hodgson, "The Infrared properties of Bismuth," Cambridge Univ. Letter to Editor (1953).

[56] R. Tediosi, N. P Armitage, E. Giannini, D. Van der Marel, "Charge carrier interaction with a purely electronic collective mode: Plasmarons and the infrared response of elemental Bismuth," Phy. Rev. Lett, **99**, 16406-4, (2007).

[57] K. Lee, A. J. Heeger, and Y. Cao, "Reflectance of polyaniline protonated with camphor sulphonic acid: Disorder metal-insulator boundary," Phys. Rev. B **48**, 14884-91, (1993).

[58] K. Lee, R. Menon, C. O. Yoon, A. J. Heeger, "Reflectance of conducting polypyrrole: Observation of the metal-insulator transition driven by disorder," Phys. Rev. B, **52**, 4779-4787, (1995).

[59] K. Lee, S. Cho, S. H Park, A. J. Heeger, "Metallic transport in polyaniline," Nature **441**, 65-68, (2006).

[60] M. G Han, J. Lee, S. W. Byun, S. S. Im, "Physical properties and thermal transition of polyaniline film," Synth. Met. **124**, 337-343, (2001).

[61] A. A. Syed, M. K. Dinesan, "Polyaniline a novel polymeric material," Talanta **38**, 815-837, (1991).

[62] B. E Shawn, V. Tito, "Graphite/Polyaniline (GP) Composites: synthesis and characterization," Carbon **43**, 2983-2988, (2005).

[63] S. Bourdo, Z. A. Li, S. B. Alexandru, F. Watanbe, V. Tito, and I. Paval, "Structural, Electrical, and Thermal Behavior of Graphite-Polyaniline Composites with Increased Crystallinity," Adv. Funct. Mater. **18**, 432-440, (2008).

[64] E. J. Fischer, "Graphite intercalation compounds: Electronic properties and their correlation with chemistry," Physica B+C **99**, 383-394, (1980).